Influences of Acid on Molecular Forms of Fluorescein and Photoinduced Electron Transfer in Fluorescein-Dispersing Sol−Gel Titania Films

Hiromasa Nishikiori*[1], Rudi Agus Setiawan[1], Kyohei Miyashita[1], Katsuya Teshima[1], and Tsuneo Fujii[2]

[1]Department of Environmental Science and Technology, Graduate School of Science and Technology, Shinshu University, 4-17-1 Wakasato, Nagano 380-8553, Japan

[2]Nagano Prefectural Institute of Technology, 813-8 Shimonogo, Ueda, Nagano 386-1211, Japan

*Corresponding author e-mail: nishiki@shinshu-u.ac.jp (Hiromasa Nishikiori)

ABSTRACT

Fluorescein-dispersing titania gel films were prepared by the acid-catalyzed sol−gel reaction using a titanium alkoxide solution containing fluorescein. The molecular forms of fluorescein in the films, depending on its acid–base equilibria, and the complex formation and photoinduced electron transfer process between the dye and titania surface were investigated by fluorescence and photoelectric measurements. The titanium species were coordinated to the carboxylate and phenolate-like groups of the fluorescein species. The quantum efficiencies of the fluorescence quenching and photoelectric conversion were higher upon excitation of the dianion species interacting with the titania, i.e., the dye–titania complex. This result indicated that the dianion form was the most favorable for formation of the dye–titania complex exhibiting the highest electron transfer efficiency. Using nitric acid as the catalyst, the titania surface bonded to the fluorescein instead of the adsorbed nitrate ion during the steam treatment. The dye–titania complex formation played an important role in the electron injection from the dye to the titania conduction band.

Keywords: fluorescein; acid–base equilibria; fluorescence; photoinduced electron transfer; photoelectric conversion; titania; sol–gel method; complex formation

INTRODUCTION

Photons can be controlled to be efficiently absorbed and emitted by dye molecules having specific π-conjugated systems. Xanthene dyes as laser dyes are available materials for utilizing photoenergy due to their high absorption and fluorescence efficiencies in various visible light regions (1). Nanocomposite films consisting of organic dye molecules and an inorganic matrix are expected to be applied to electronic devices such as photovoltaic cells (2−4). The sol−gel method enables the production of glasses and ceramics via hydrolysis and polycondensation reactions of metal alkoxides at a lower temperature than for the solid phase method (5−7). The organic−inorganic hybridization is performed by mixing the organic compounds into the starting solution. The sol−gel coating is a useful way to easily provide such highly functional materials to the inactive plate surface (5−9). The molecular-order physicochemical properties of the systems should vary according to the progress of the sol−gel reaction. The variations are interesting and important for understanding the fundamental chemical reactions. The absorption and fluorescence spectral measurements elucidate the behavior of the organic molecules in the sol−gel reaction system (10−14). Previous studies have revealed the relationships between the physicochemical changes during the sol−gel−xerogel transitions and the spectroscopic properties of the organic dyes; i.e., rhodamine B (15,16), methylene blue (17), and 9-aminoacridine (18), in the silicon alkoxide systems.

Many scientists have investigated the electron donor−acceptor interaction between the dye molecules and the titania in the dye−titania systems used for the dye-sensitized solar cells (DSSCs) (3,4,19−28). It was reported that xanthene dye molecules formed a chelate complex with the titanium species on the titania surface in the dye−titania systems (3,19,20,23−25). The complex formation induces an interaction between their orbitals and the red-shift in their absorption spectrum. This interaction caused the ligand-to-metal

charge transfer (LMCT) interaction and a fast-electron injection into the titania conduction band (3,23,24).

We have investigated the photoelectric conversion properties of the dye-dispersing titania gel, which is prepared from a titanium alkoxide sol containing the dye molecules and is different from the conventional dye-adsorbed titania (29−37). The high dispersion of the dye molecules into the titania provides the strong dye−titania interaction. The gel was presumed to consist of amorphous, nanosized, and particle-like units, which have a semiconductor-like quasi-conduction band structure with a low density of states. The dye molecules exist in the nanopores of the gel. Furthermore, the effect of the hydrothermal treatment on their photoelectric conversion properties has also been investigated because it is an effective method to crystallize the amorphous phase and improve the photoelectric conversion performance (29−37). It was reported that the crystallization of amorphous titania to anatase was achieved by a hydrothermal treatment at a low temperature because water molecules catalyzed the rearrangement of the TiO_6 octahedra (38).

In a further study, the steam treatment enhanced the photoelectric conversion efficiency of the fluorescein-dispersing titania gel due to not only crystallization of the titania gel, but also the dye–titania surface complex formation (31−37). Based on the results of the time-resolved spectroscopy and photoelectric measurements, the electron injection process from the dye excited states to the titania conduction band is important for the photoelectric conversion. The dye-dispersing titania gel is an interesting material for the basic study of DSSCs because the conditions of the preparation and hydrothermal treatments cause the changes in the titania structure and the dye–titania bond character. The investigation of the dye−titania interaction in this system will result in determining new information expected to be applicable to some optical and electronic devices.

The dye aggregation on the titania surface is a serious problem of the conventional DSSCs because it suppresses the electron injection (39−41). Unlike the interaction between the dye molecules, the interaction between the dye molecule and the titania surface is favorable for the electron injection. It is important that the dye and titania surface species are controlled in order to provide effective dye−titania interaction without stacking on the surface. In our dye-dispersing titania systems, the dye molecules can be highly dispersed on the surface of the individual titania nanoparticles without their aggregation. Therefore, our previous study indicated that the shapes of the absorption and photocurrent spectra of the fluorescein- and eosin Y-dispersing titania films only slightly changed and their absorbance and photocurrent values proportionally increased with an increase in the dye concentration (37). The internal quantum efficiency of the photoelectric conversion was higher than that of the conventional dye-adsorbing titania electrodes in which the dye molecules were easily aggregated, thus deactivated by the energy transfer (33,34,37). The complex formation between fluorescein and titania depends on the acid−base equilibria of the molecule with the carboxyl and hydroxyl groups. The structures of fluorescein species are shown in Scheme 1. The complex formation is also affected by the coexisting ions. In this study, the fluorescence spectroscopic and photoelectric measurements of the dye-dispersing titania films were conducted in order to determine new information about the dye−titania chemical and electronic interactions. The measurements will reveal the influence of adding acid, i.e., nitric acid, hydrochloric acid, or sulfuric acid, to the starting solution on the molecular forms of the dye, the chemical interaction between the dye molecule and the titania surface, and the electron injection from the dye to the titania.

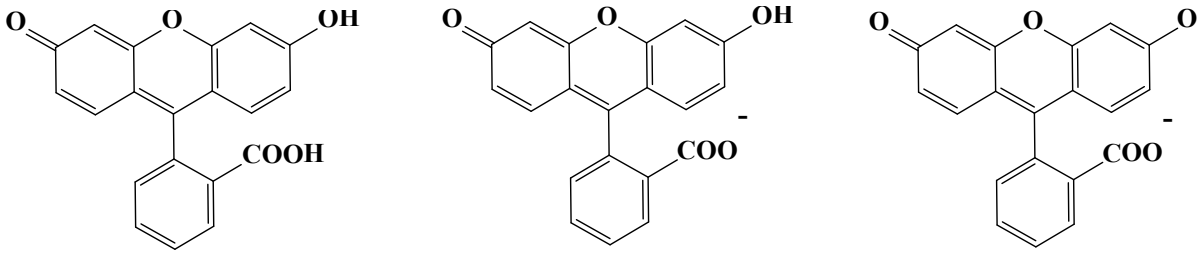

Neutral Anion Dianion

Scheme 1. Structures of fluorescein species.

MATERIALS AND METHODS

Materials. Titanium tetraisopropoxide, ethanol, fluorescein, hydrochloric acid, nitric acid, sulfuric acid, diethylene glycol, iodine, lithium iodide, and sodium hydroxide (Wako Pure Chemical Industries, S or reagent grade) were used without further purification. Water was ion-exchanged and distilled. Glass plates coated with the ITO transparent electrode (AGC Fabritech) were soaked in hydrochloric acid (1.0 mol dm^{-3}) for 2 h and then rinsed with water. The electrolyte used for the electrical measurements consisted of a diethylene glycol solution of iodine (5.0×10^{-2} mol dm^{-3}) and lithium iodide (0.50 mol dm^{-3}).

Preparation of electrodes. The sol–gel reaction systems were prepared by mixing 5.0 cm^3 of titanium tetraisopropoxide, 25.0 cm^3 of ethanol, 0.21 cm^3 of water, and an acid as the catalyst of the sol–gel reaction. The systems containing 7.5×10^{-3}, 7.5×10^{-2}, and 7.5×10^{-1} mol dm^{-3} of nitric acid were labeled SG-1N, SG-2N, and SG-3N, respectively. The systems containing 7.5×10^{-2} mol dm^{-3} (equivalent concentration) of hydrochloric acid and sulfuric acid were labeled SG-2H and SG-2S, respectively. Fluorescein was individually dissolved into SG-1N, SG-2N, SG-3N, SG-2H, and SG-2S in which its concentration was 1.0×10^{-2} mol dm^{-3} and these systems were labeled SG-1NF, SG-2NF, SG-3NF SG-2HF, and SG-2SF, respectively. The dip-coated thin films were prepared from the systems in which the sol–gel reaction proceeded for 1 day to prepare the electrodes.

In order to prepare the electrode samples coated with the crystalline titania, the glass plates with the ITO transparent electrode were dip-coated in the dye-free system, SG-2N, and then heated at 773 K for 30 min. These electrodes were labeled E-0. Furthermore, the working electrodes were prepared in which the E-0 was dip-coated with SG-1NF, SG-2NF, SG-3NF, SG-2HF, or SG-2SF. These working electrodes were labeled WE-1NF, WE-2NF, WE-3NF, WE-2HF, and WE-2SF, respectively. The glass plates without ITO were also coated with SG-1NF, SG-2NF, SG-3NF, SG-2HF, or SG-2SF in order to obtain their XRD patterns and spectroscopic information. These film samples were labeled F-1NF, F-2NF, F-3NF, F-2HF, and F-2SF, respectively.

The steam-treatment effects on the XRD patterns and spectroscopic and photocurrent properties of the samples were investigated. Water was heated at 373 K and the electrode and XRD samples were exposed to its steam for 120 min. The steam pressure was about 100 kPa. The steam-treated samples were additionally labeled "-s", such as WE-1NF-s, WE-2NF-s, and WE-3NF-s.

Measurements. The crystalline phase of the film samples was determined using an X-ray diffractometer (Rigaku RINT-2200V). The layer thickness of the electrode samples was estimated from their cross section using a field emission scanning electron microscope (Hitachi S-4100). The UV-visible absorption and fluorescence spectra of the prepared film samples were observed using a spectrophotometer (Shimadzu UV-3510) and a fluorescence spectrophotometer (Shimadzu RF-5300), respectively. Raman scattering due to the titania gels was subtracted from the observed fluorescence spectra. The reflection spectra of the films with and without the dye were also obtained by the fluorescence spectrophotometer, and then the net absorption was calculated. The fluorescence quantum yield was estimated using the absorption and fluorescence intensities of the dye in the films. The amounts of

the dyes existing in the electrode samples were estimated from the absorption spectra of the dyes eluted by the 0.1 mol dm^{-3} sodium hydroxide aqueous solution.

The flakes of the dye-dispersing film samples were pressed in the KBr pellets and their IR spectra were taken using an FTIR spectrophotometer (Shimadzu IRPrestige-21). The XPS spectra were observed by AlKα radiation using an X-ray photoelectron spectrophotometer (ULVAC PHI 5600) in order to estimate the amounts of the acids remaining in the film samples.

The iodine-based electrolyte was allowed to soak into the space between the electrode sample and the counter Pt electrode. For the spectroscopic measurements, the electrodes was irradiated by monochromatic light with each wavelength obtained from the fluorescence spectrophotometer by a 150 W Xe short arc lamp (Ushio UXL-155). During the light irradiation, the short circuit currents of the electrodes were measured by a digital multimeter (ADCMT 7461A). The I–V curves of the electrodes were measured by a potentiostat (Hokuto Denko HSV-100) during the irradiation by visible light at a wavelength longer than 400 nm emitted by the 150 W Xe short arc lamp using a sharp cut filter. The intensity at each wavelength of the light source was obtained using a power meter (Molectron PM500A) in order to estimate the incident photon-to-current conversion efficiency (IPCE) and quantum efficiency for the photocurrent from the excited dye in the electrode samples. The visible absorbance of the present electrode samples was lower than 1.0 which was sufficient to measure the number of absorbed photons in order to calculate the quantum efficiency.

RESULTS AND DISCUSSION

Microscopic morphology of the samples

The untreated titania gel film had a structureless morphology and seemed amorphous (not shown). Figure 1 shows the SEM images of the dye-containing titania films steam-treated

for 120 min. F-1NF-s and F-2NF-s consisted of 10–20 nm particles as previously reported (29,34,35). On the other hand, smaller-sized particles, ca. 5 nm, were observed in the F-3NF-s prepared from the sol containing the highest acid concentration. This is because acid promotes the hydrolysis of titanium alkoxide and inhibits its polycondensation and particle growth. The particle size was changed by such reaction conditions. The thickness of the dye-containing layer of the dye-dispersing titania gels was ca. 350 nm as previously reported (32−37).

Figure 1

No peak is observed in the XRD patterns of the untreated amorphous gel films. The XRD patterns of the steam-treated films are shown in Figure 2. A peak at around 25° was observed only in F-2NF-s, indicating that an anatase-type crystal was produced in the film, whereas F-1NF-s and F-3NF-s had no such diffractive peak. The size of the crystallites of the film was estimated from its full-width at half-maximum of the 25° peak using Sherrer's equation, $D=0.9\lambda/\beta\cdot\cos\theta$. The size was 5.8 nm for F-2NF-s and much smaller than that of the crystalline titania foundation, ca. 18 nm, as previously shown (32−37). A small amount of acid decreased the rate of the crystal growth because hydrolysis of the titanium species did not effectively proceed and followed by the rearrangement of the TiO_6 octahedra. A large amount of titania crystal nuclei were produced in the gel prepared from the sol containing a highly concentrated acid because many small structural units were formed in the untreated gel, in which the acid controlled the polymerization and particle growth.

Figure 2

Influence of acid on absorption and fluorescence spectra

Figure 3 shows the FTIR spectra of the untreated and stream-treated films. Generally, the peaks of the carboxyl C=O stretching and the carboxylate COO^- antisymmetric and symmetric stretching vibrations are observed at 1710, 1597, and 1391 cm^{-1} in the fluorescein,

respectively (33,42). In addition, the bands at around 1557 and 1464 cm^{-1} are assigned to the quinone-like C=O and C=C stretching vibration (33,42). The untreated F-1NF exhibited carboxylate bands at 1580 and 1400 cm^{-1} and the quinone-like bands at 1540 and 1450 cm^{-1}. The band observed at 1383 cm^{-1} is due to NO_3^-. This band intensity corresponded to the nitrogen amount estimated by XPS analysis. The significant shifts in the carboxylate and quinone-like bands are due to the interaction between the functional groups and the titanium species of titania. With respect to F-1NF, the carboxylate band at 1580 cm^{-1} and the quinone-like (phenolate-like) band at 1450 cm^{-1} were shifted to ca. 5 cm^{-1} lower wavenumber by the steam treatment due to the enhancement of the interaction between the functional groups and the titanium species of titania as previously shown (33). The carboxyl band was also slightly observed at around 1700 cm^{-1} in F-2NF and clearly in F-3NF before the steam treatment. The quinone-like band intensity at 1540 cm^{-1} was relatively stronger in the films prepared from the sols with a higher acid concentration. These results indicated the acid-base equilibria of fluorescein with the carboxyl and hydroxyl groups. A more acidic titania was prepared from the sols with a higher concentration of the acid, which produced the Brønsted acidic hydroxyl groups on the titania particle surface as previously reported (43,44). The relative intensities of the carboxyl and quinone-like bands decreased and that of the interacting carboxylate and phenolate-like bands increased by the steam treatment (33). The NO_3^- band intensity decreased by the steam treatment due to its evaporation. The interactions between the carboxylate and phenolate-like groups of fluorescein and titanium species relate to the complex formation between the dye and titania surface (31−37). A higher amount of the complex is expected to be formed in the lower acidic film containing a higher amount of the dianion. The proton dissociation constants, pK_a values, of the carboxyl and hydroxyl groups of fluorescein are 4.45 and 6.80, respectively

(45). The dianion form was stabilized by its interaction with the positive sites on the titania surface even though the titania surface was generally acidic (3,19,20,23−25, 46).

Figure 3

A broad band at around 3300 cm^{-1} were observed in the untreated and steam-treated titania samples as shown in Figure S1 (see Supporting Information) and assigned to the O–H stretching of the TiOH group and adsorbed H_2O. This spectral shape was slightly changed by the acid concentration or steam treatment. The peak of the O–H stretching band for the steam-treated titania was seen at a wavenumber somewhat higher than that for the untreated sample. In our previous study, the O 1s peaks of the XPS spectra were observed at 530.1 eV in the untreated sample, and these were almost the same as those of the steam-treated samples (35). The spectrum for the untreated sample was broader than the steam-treated samples due to a large amount of hydroxyl groups exhibiting the peak at around 531.0–531.5 eV. The spectrum for the steam-treated sample also has a shoulder at around 532 eV assigned to the adsorbed water molecules. This indicated that a larger amount of the water molecules was physically adsorbed on the steam-treated sample.

The complex formation between fluorescein and titania depends on the acid−base equilibria of the molecule. We should clarify the influence of adding acid to the sol−gel starting solution on the dye−titania complex formation and the electron injection in the dye-dispersing titania. Figure 4 shows the visible absorption spectra of the sols, SG-1NF, SG-2NF, and SG-3NF, before the film preparation and the constituent spectra of the fluorescein species separated from the spectra of the fluorescein-containing sols. The molar extinction coefficient values of the fluorescein species were assumed to be equal to those in aqueous solutions (47). Based on the acidity dependence of the absorption spectra, the peaks at 445, 484, and 511 nm were assigned to the neutral, anion, and dianion species of fluorescein, respectively. The neutral, anion, and dianion species exhibit a peak at 434 nm, 453 and 472

nm, and 490 nm in aqueous solutions, respectively (47). The red-shifts observed in the titania systems indicated the strong interaction between the dye species and titanium species such as the titanium alkoxide polymer and very small titania particle, i.e., the dye–titania complex formation (33,36). The absorption spectrum of the dianion species in the titania systems was regarded as that of the dianion−titania complex. The spectra observed in the basic (ca. pH 7.5) and acidic (ca. pH 2) sols were regarded as those of the dianion and neutral species, respectively. The spectrum of the anion species was obtained by subtracting the dianion spectrum from the spectrum observed in the sol of ca. pH 6.

Figure 4

Figure 5 shows the visible absorption spectra of the untreated films, F-N1F, F-N2F, and F-N3F, and the stream-treated ones, F-N1F-s, F-N2F-s, and F-N3F-s. The concentrations of the fluorescein species in the films were estimated by spectral curve fitting of the sum of the constituent spectra (Figure 4b) multiplied by coefficients to the observed spectra as shown in Table 1 and Figure S2 (see Supporting Information). The total dye concentrations in the films corresponded to the values obtained from their elution. The peaks of the absorption spectra of F-N1F, F-N2F, and F-N3F were located at 485, 472, and 475 nm, respectively. The amounts of the neutral and anionic species were lower than those in the sols because the systems were neutralized by acid evaporation and further polymerization of the titanium species during the dip-coating. The absorbance values of these samples were higher in the order of F-1NF, F-2NF, and F-3NF, because the interactions between the carboxylate and phenolate-like groups of fluorescein and titanium species were promoted in the lower acidic sol or film during the dip-coating. The absorbance of these samples decreased and the bands were red-shifted and broadened by the steam treatment. Some amount of water vapor was condensed into liquid on the titania film during the steam treatment, and then some of the fluorescein molecules adsorbed on the titania pore surface were desorbed into the liquid

water phase. The total amount of the dye molecules which remained in the titania films after the steam treatment and those which were desorbed into the water phase was nearly equal to that of the dye in the titania films before the steam treatment (33). An only slight amount of the dye molecules were decomposed during the steam treatment although they were decomposed by heating at more than 573 K. The peaks for F-1NF-s, F-2NF-s, and F-3NF-s were located at 490, 480, and 480 nm, respectively. This result indicated that the nitric acid was removed and the dye interacted with the titania. The absorbance values of the steam-treated samples were higher in the order of F-2F-s, F-1NF-s, and F-3NF-s. This depends on the solubility of fluorescein in water under each acidity condition, i.e., the solubility in more basic water is higher. Consequently, the order of the more soluble species is the dianion, anion, and neutral species. The absorbance of F-2NF-s was higher than that of F-1NF-s because a higher amount of the fluorescein species remained in the film. The absorbance of F-3NF-s was lower than that of F-2NF-s due to the weakest interaction of the neutral species with the titania rather than its solubility in water. The relatively higher amount of the dianion species was in the samples prepared from the sol with a lower acid concentration. F-1NF-s contained the highest percentage of the dianion in the three samples. The band at the wavelength longer than 500 nm can be assigned to the fluorescein dianion−titania complex as shown in Scheme 2 (33,36). The anion species bonds with the titanium species through only the carboxylate group, whereas the dianion species more strongly bonds to them through the carboxylate and phenolate-like groups. The FTIR analysis also indicated that the steam treatment enhanced the interaction of the carboxylate and quinone-like groups with the titanium species as shown in Figure 3. Our previous study indicated that the xanthene dyes with only the carboxylate group more weakly interacted with the titania and exhibited a lower electron injection efficiency than those with the carboxylate and quinone-like groups (48). The interaction between the orbitals of the

dye molecule and titania caused the red-shift in the absorption spectrum. Therefore, the formation of the dianion−titania complex more significantly changed the absorption spectrum than the interaction between the anion and titania. The stream treatment promoted the interaction and complex formation between the dianion species and titania although it induced the fluorescein species weakly interacting with the titania to be desorbed into the water phase. The FTIR or UV-vis spectral behavior due to the complex formation was not observed in the conventional dye-adsorbed titania (33).

Figure 5 and Table 1

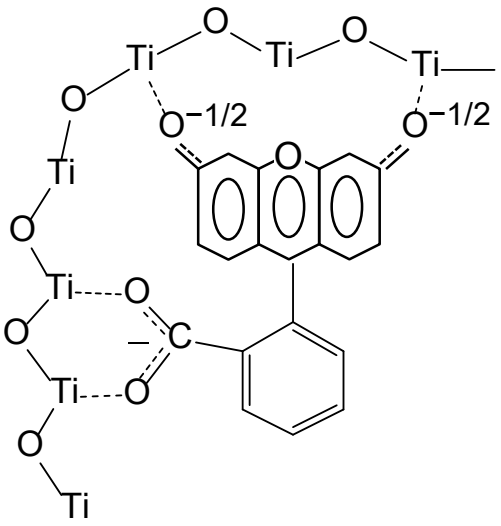

Scheme 2. Structure of fluorescein dianion−titania complex.

In our previous study, the dye molecules were finely dispersed in the dye-dispersing titania films compared to the conventional dye-adsorbing materials (37). The concentrations of fluorescein adsorbed on the crystalline titania films from the 1.0×10^{-3}, 5.0×10^{-3}, and 1.0×10^{-2} mol dm^{-3} fluorescein ethanol solutions were 2.7×10^{-2}, 4.0×10^{-2}, and 5.5×10^{-2} mol dm^{-3}, respectively. The dye molecules were easily aggregated in the dye-adsorbing titania films. The dye concentrations in the present titania films after the steam treatment were the same order of magnitude as those in the dye-adsorbing films or greater. However, the dye

molecules were highly dispersed on the surface of the individual titania nanoparticles without their aggregation.

Figure 6 shows the fluorescence spectra of the untreated samples, F-1NF, F-2NF, and F-3NF, and stream-treated samples, F-1NF-s, F-2NF-s, and F-3NF-s. A fluorescence peak was observed at around 530−540 nm, assigned to the dianion, in F-1NF and F-2NF, and at 520 nm, assigned to the anion, in F-3-NF, depending on the acidity in the films (47). Most of the anion species are deprotonated to form the dianion species in the excited states and emit a fluorescence because the proton dissociation constant in the excited states, pK_a* value, is ca. 6.0 lower than that in the ground state, pK_a value, 6.8 (49). The spectrum was red-shifted by the steam treatment of F-1NF due to acid evaporation. The fluorescence quantum yields of the samples were estimated from their absorption and fluorescence spectra as shown in Figure 7. The fluorescence quantum yields of the untreated and steam-treated samples were higher in the order of F-3NF, F-2NF, and F-1NF, and F-3NF-s, F-2NF-s, and F-1NF-s, respectively. These orders can depend on the complex formation ability of the fluorescence species related for the electron transfer process. It is important that the fluorescence quantum yields of the steam-treated samples were lower than those of the untreated samples. This result indicated that some fluorescein species formed a complex with the titania surface, which were strongly quenched on the titania surface by the electron injection to the titania conduction band.

Figure 6 and Figure 7

The fluorescence lifetime of the fluorescein anion and dianion was reported to be ca. 3−4 ns (49,50). The electron injection from the excited dye to the titania was reported to occur within 100 ps (51−53). The steady state fluorescence is completely quenched by the electron injection from the dye into the titania (23,24). This was enhanced by the dye–titania complex formation based on a previous time-resolved spectroscopic study (36). The

film containing a higher amount of the dianion, which is the most negative species and presumed favorable for the ligand, was more strongly quenched although the fluorescence quantum yield of the dianion is higher than those of the other species (49). It was previously reported that the observed fluorescence mainly originated from the dye molecules weakly adsorbed on the titania nanoparticle surface with the lifetime of 0.22−0.41 ns (36). The fluorescence observation was more sensitive to the complex formation than the FTIR and visible absorption analyses.

Actually, the fluorescence decay curves of the present dye-dispersing titania consist of two components with the lifetimes of 0.20–0.43 and 3.3–3.7 ns as shown in Figure S3 and Table S1 (see Supporting Information). Table S1 shows the fluorescence intensities just after excitation, i.e., the maximum intensities, and fitting parameters. These values are close to those reported for the dye-adsorbing titania systems (24). The longer lifetime component is assigned to the original anion or dianion. The shorter lifetime component can be assigned to the fluorescence of the dye interacting with the titania, which is caused by the recombination between the injected electron and the dye (24). Our previous study indicated that the electron injection occurred within a few picoseconds and the recombination between the injected electron and the dye occurred within 20 ps (31). It is reasonable that the reproduced excited-states of the dye exhibited the fluorescence with the lifetimes of 0.20–0.43 ns in the present systems. In all the films, the exponential function factor for the shorter lifetime component, A_1, was much higher than that for the longer lifetime one, A_2. The dye somewhat interacted with the titania and exhibited a photoinduced electron transfer to the titania even in the untreated film. The A_1 value slightly increased with a decrease in the acidity and by the steam treatment. The lifetime of the shorter lifetime component decreased with a decrease in the acidity and by the steam treatment, indicating that the dianion−titania complex can have a shorter lifetime. On the other hand, the maximum

fluorescence intensity clearly decreased with a decrease in the acidity and by the steam treatment. The yield of the electron injection from the dye to the titania can have an inverse relation to the fluorescence maximum intensity because the electron injection is reported to occur within 100 ps (51−53). In this study, the enhancement of the interaction between the dye and titania, which increased the electron injection yield, indicated the dianion−titania complex formation.

Influence of acid on photoelectric conversion properties

The IPCE spectra of the untreated and stream-treated electrodes are shown in Figure 8. The photocurrent in the UV region resulted from the titania band-gap excitation. The IPCE values in the UV region slightly depended on the acid concentration in the sol for the sample preparation and slightly increased by the steam treatment. This is because the crystalline titania layer was formed under the dye-dispersng titania layer. Furthermore, the electron transport efficiency or electron conductivity did not reflect the titania crystallinity because the electrons can be transported on the titania particle surface rather than in the bulk in such a low crystalline titania (54). It was reported that the electrical resistance of the untreated titania gel film (amorphous), steam-treated titania gel film (crystallite size: ca. 5 nm), and the crystalline titania film (crystallite size: ca. 18 nm) were 6.8×10^5, 8.1×10^4, and 3.1×10^4 Ω cm, respectively (35). In the photoelectric conversion measurement, the steam-treated titania electrodes exhibited a 70% efficiency compared to the electrodes having the crystalline titania. The electrical conductivity of the steam-treated film was close to that of the crystalline titania film, independent of their resistivity. The electrical conductivity of the crystalline titania electrode coated with the untreated titania gel film was also very close to that of the electrode coated with the steam-treated film (34).

Figure 8

The IPCE values in the visible region for the untreated electrodes, WE-1NF, WE-2NF, and WE-3NF, were higher in the order of their absorbance due to the fluorescein species. In spite of the absorbance decrease (Figure 5), the photocurrent of all the electrodes increased due to the 120-min treatment, while the peaks were red-shifted to around 500 nm. It was reported that the growth and crystallization of the particles and the decrease in the defect density by the steam treatment improved the electric conductivity (29,30,32−35). However, the present results suggest that the increase in the IPCE values is due to an increase in the chelate complex between the fluorescein and the titania (the around 500 nm species) rather than improvement of the electric conductivity of the titania gel. The adsorbed water molecules enhanced the mobility of the charge carriers on the surface. The steam treatment enhanced not only the electric conductivity of the titania, but also the dye−titania interaction that plays an important role in generating the photocurrent in this system. The IPCE values of the steam-treated electrodes were higher in the order of WE-2NF-s, WE-1NF-s, and WE-3NF-s corresponding to their absorbance values. In our previous study, the open circuit voltage as well as the short circuit current was increased by the dye−titania complex formation, which caused a negative shift in the titania conduction band potential due to the negative charge of the dye molecule (33).

The quantum efficiency of the photoelectric conversion for each electrode was estimated in order to clarify the contribution of the species to the photocurrent. Figure 9 show the quantum efficiency at each wavelength for the untreated and stream-treated electrodes. The quantum efficiency of WE-1NF was higher than those of the other two electrodes due to containing the higher amount of the dianion species although the amount of the dianion species in the electrodes was much lower than those of the neutral and anion species. Therefore, the dianion species is expected to exhibit the very highest electron injection efficiency. The higher efficiency was found at the longer wavelength (500−510 nm) for all

the electrodes, indicating that the dianion species absorbing longer wavelength light more efficiently injected the excited electrons than the neutral and anion species. The quantum efficiency for all the electrodes was significantly increased by the steam treatment. The higher efficiency was also obtained at the longer wavelength for the stream-treated electrodes. The absorption band located at the wavelength longer than 500 nm can be the fluorescein dianion–titania complex significantly contributed to the photocurrent.

Figure 9

These values were much lower than those of the general dye-sensitized solar cells because the very thin titania films were used for the semiconductor layers in the present electrodes in order to obtain their exact absorbance and quantum efficiency. The IPCE at 500 nm, 17%, and internal energy conversion efficiency, 1.1%, were obtained using a thicker titania electrode coated with such a fluorescein-dispersing titania film in a previous study (55).

Influence of acid on the interaction between the dye and titania surface

The characterization of the samples prepared using hydrochloric acid and sulfuric acid was also conducted in order to examine the interaction between the dye and titania surface. The SEM images, XRD patterns, and FTIR spectra of the samples prepared using hydrochloric acid and sulfuric acid are shown in Figure S4, Figure S5, and Figures S6 and S7, respectively (see Supporting Information).

The particle size of WE-2HF-s and WE-2SF-s was 10−20 nm, similar to that of WE-2NF-s. The XRD patterns of F-2HF-s and F-2SF-s were also similar to that of F-2NF-s because they were prepared from the sols containing the same concentration of the acids. The crystallite sizes of F-2NF-s, F-2HF-s, and F-2SF-s were 5.8, 5.7, and 5.3 nm, respectively. The FTIR spectrum of F-2SF exhibited an absorption increase at 1300−1000 cm^{-1} due to the SO_4^{2-} bands at 1135 and 1048 cm^{-1} and the HSO_4^- band at 1234 cm^{-1} (56,57). These band intensities corresponded to the sulfur amount estimated by XPS analysis. The bands

remained after steam treatment due to their nonvolatile property, whereas the NO_3^- band disappeared after the treatment in the nitric acid system. The carboxylate band at 1580 cm^{-1} and the quinone-like band at 1450 cm^{-1} were shifted to lower wavenumber by the steam treatment due to the enhancement of the interaction between the functional groups and the titanium species of titania (33). Hydrochloric acid does not remain in the film because it should evaporate during the film preparation. No chlorine species was detected in the untreated and steam-treated films by XPS analysis.

The band at around 3300 cm^{-1} assigned to the O–H stretching were observed in the untreated and steam-treated titania samples as shown in Figure S7 (see Supporting Information). The O–H band intensity of F-2HF was stronger than that of the others because the anions slightly remained on the titania surface. The spectra were slightly changed by the steam treatment.

Figure S8 shows the visible absorption spectra and the separated constituent spectra of the untreated and steam-treated films prepared using different acids (see Supporting Information). The concentrations of the fluorescein species in the films were estimated as shown in Table S2 (see Supporting Information). In all the systems, the absorbance decreased by the steam treatment due to the dye desorption into the water phase. Especially, the value significantly decreased in the sulfuric acid system because the dye molecules did not interact with the titania surface covered with SO_4^{2-} and HSO_4^-. In the hydrochloric acid system, the decrease in the absorbance during the steam treatment was smaller than those in the other systems due to the titania surface covered with a high amount of the OH group, with which the dye molecules somewhat interact. The amount of the dianion species in F-2NF-s was higher than those in F-2HF-s and F-2SF-s although those in all the untreated samples were similar.

Figure S9 shows the fluorescence spectra of the untreated and steam-treated films prepared using different acids (see Supporting Information). The fluorescence intensity was higher in the order of F-2SF, F-2HF, and F-2NF before treatment. This result indicated that the main fluorescein species, the anion species, was slightly quenched by the interaction with the titania and readily emitted in the film. The relative amount of the fluorescent anion species in F-2SF was higher than those in F-2HF and F-2NF. In lower acidic F-2HF and F-2NF, most of the anion species were deprotonated to form the dianion species in the excited states and emitted a fluorescence, which was quenched by the interaction with the titania. The negative ion species (SO_4^{2-} and $HSO_4^{-)}$ inhibited the interaction between the dye and titania surface. The fluorescence intensity of F-2NF-s was lower than that of F-2HF-s after the steam treatment due to the desorption of nitrate ions and occurrence of the interaction. A weak fluorescence was observed in F-2SF-s because a great number of the dye molecules were desorbed after the steam treatment.

Figure S10 shows the IPCE spectra of the untreated and steam-treated electrodes (see Supporting Information). The IPCE values of WE-2SF in the UV region were higher than those of the other untreated samples. The IPCE values of the untreated samples in the UV region were higher in the order of WE-2SF, WE-2NF, and WE-2HF. This order indicated the amount of the ionic species on the titania surface because the electrons can be transported on the titania particle surface rather than in the bulk in such a low crystalline titania (54). The electron transport efficiency or electron conductivity in the bulk of the samples should be similar. The IPCE values of the steam-treated samples in the UV region were similar due to similar crystallinity of the titania. The order of the IPCE values of the samples in the visible region was very different from that of their fluorescence intensities. The IPCE values of WE-2NF and WE-2HF in the visible region were higher than those of WE-2SF.

The IPCE values of the steam-treated samples were higher in the order of WE-2NF-s, WE-2HF-s, and WE-2SF-s.

Figures 10 and 11 show the fluorescence quantum yields of the untreated and steam-treated films and photocurrent quantum efficiency of the electrodes prepared using different acids, respectively. A schematic diagram of the change in the interaction between the dye and titania surface is shown in Scheme 3. It is suggested that the untreated dye-dispersing titania gel film consists of the amorphous, nanosized, and particle-like units, which have a semiconductor-like quasi-conduction band structure with a low density of states, and the quasi-conduction band accepts electrons from the excited dye molecules. The formation of anatase-type titania nanocrystals by the rearrangement of the TiO_6 octahedra during the steam treatment leads to the formation of the conduction band with higher density of acceptor states and therefore increases the electron injection rate. An increase in the overall crystallinity of titania nanoparticles results in an increase in the surface quality of the nanoparticles, which improves the anchoring geometry of the dye on their surfaces. The favorable anchoring geometry of the dye also causes the faster electron injection (31).

The fluorescence quantum yield was higher in the order of F-2SF, F-2HF, and F-2NF before the steam treatment, and F-2SF-s, F-2HF-s, and F-2NF-s after the steam treatment. The quantum efficiency of the photoelectric conversion of the samples had an inverse relation of their fluorescence quantum yield. In the hydrochloric acid system, the fluorescein molecules were adsorbed on the titania surface covered with many hydroxyl groups before and after the steam treatment. Almost all the chloride ions evaporated during the film preparation. In the nitric acid system, an excess of nitrate ions over the adsorption capacity should be removed during the film preparation and a parts of the titania surface were covered with nitrate ions before the steam treatment and then bonded to the fluorescein molecules instead of the nitrate ions after steam treatment. The fluorescein dianion, which is the most

negative species, is the most favorable of all the fluorescein species for the ion exchange. It was reported that the weak anchoring affinity of NO_3^- with titania caused rapid coordination of the titania to anionic dyes (46). In the sulfuric acid system, an excess of sulfate ions should be also removed during the film preparation. The fluorescein molecules were adsorbed on the titania surface covered with many sulfate ions before the steam treatment, and then desorbed into the water phase during the steam treatment because the sulfate ions remained on the titania surface. The fluorescein−titania complex enhanced the photocurrent and quenched the fluorescence. The fluorescein weakly adsorbed on the titania surface emitted a strong fluorescence.

Figure 10 and Figure 11

It is possible that such anions cause a negative shift in the titania conduction band and a change in the electron injection efficiency. The untreated electrodes, WE-2NF, WE-2HF, and WE-2SF, contained a large amount of the anions. However, the open circuit voltage values of the untreated electrodes were close to each other although their short circuit current density values corresponded to their IPCE values as shown in Figure S11 (see Supporting Information). This result indicated that the conduction band was slightly changed by the anions in the titania gel films.

HCl system

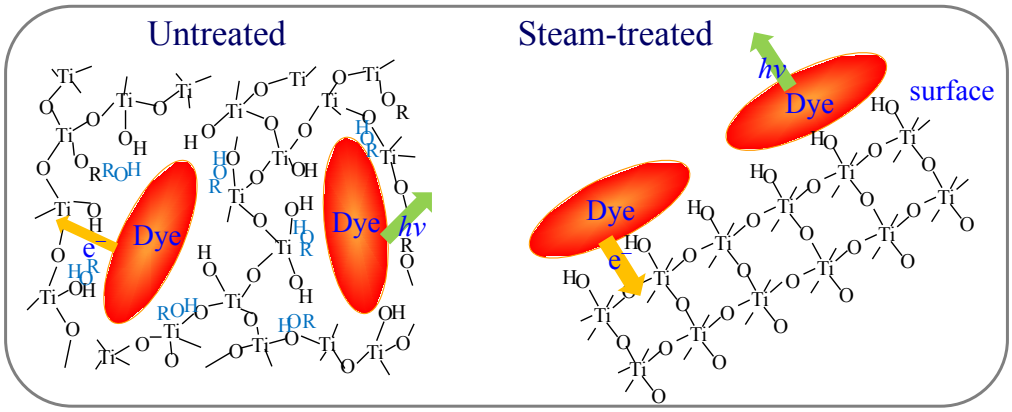

HNO_3 system

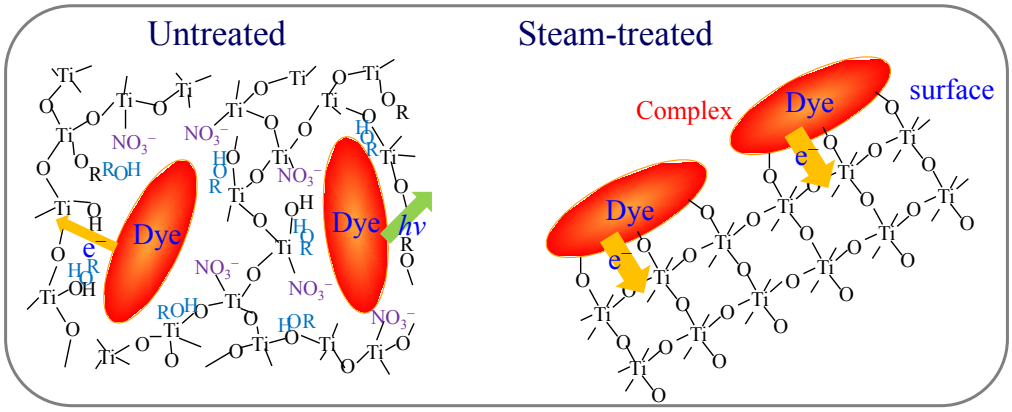

H_2SO_4 system

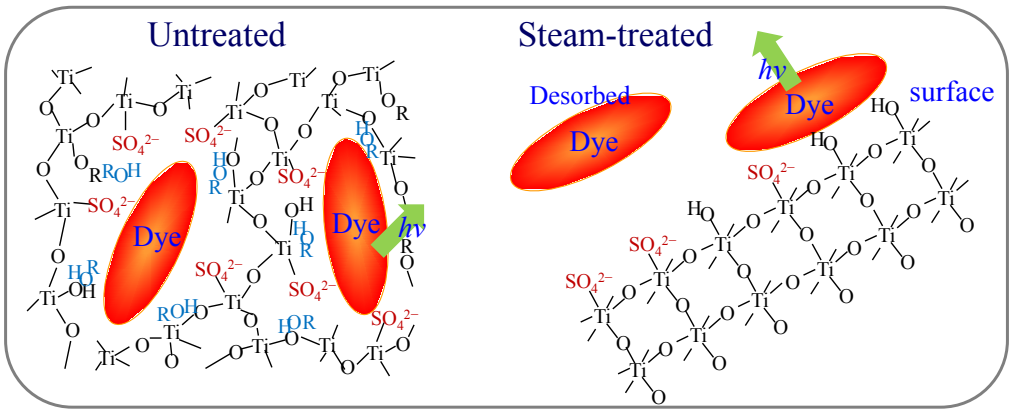

Scheme 3 Change in the interaction between the dye and titania surface during steam treatment.

Finally, the fluorescence quantum yield and quantum efficiency of photoelectric conversion for the untreated and steam-treated electrodes vs. the dianion fraction of fluorescein are shown in Figure 12. It is clear that the fluorescence quantum yield decreased and the photocurrent quantum efficiency increased with an increase in the dianion fraction. These values depended on the dianion fraction although the dianion was not major species in all the electrodes. The dianion–titania complex efficiently caused the electron injection and fluorescence quenching due to their strong chemical and electronic interaction.

Figure 12

CONCLUSIONS

Fluorescein-containing titania gel films were prepared by the acid-catalyzed sol−gel method using the titanium alkoxide solution containing fluorescein. The complex formation and electron transfer between fluorescein and the titania surface depends on the acid−base equilibria of the molecule with carboxyl and hydroxyl groups. The complex formation is also affected by the coexisting ions. Therefore, the fluorescence spectroscopic and photoelectric measurements of the dye-containing titania films were conducted in order to clarify the influence of adding acid to the starting solution on the molecular forms of the dye, the chemical interaction between the dye molecule and the titania surface, and the electron injection from the dye to the titania. The relative electron injection yield in the dye-containing titania gel film increased due to the steam treatment. The titanium species were coordinated to the carboxylate and phenolate-like groups of the fluorescein species, which was enhanced by the steam treatment. The quantum efficiency of fluorescence quenching was higher in the titania containing the dianion species interacting with the titania surface, i.e., the dye–titania complex. The quantum efficiency of photoelectric conversion was higher upon excitation of the dianion species interacting with the titania surface. These

results indicated that the dianion form was the most favorable for formation of the dye–titania complex exhibiting the highest electron injection efficiency. In the hydrochloric acid system, the fluorescein molecules were adsorbed on the titania surface covered with many hydroxide groups before and after the steam treatment. In the nitric acid system, parts of the titania surface were covered with nitrate ions before the steam treatment and then bonded to the fluorescein molecules instead of the nitrate ions after the steam treatment. In the sulfuric acid system, the fluorescein molecules were adsorbed on the titania surface covered with many sulfate ions before the steam treatment, and then desorbed into the water phase during the steam treatment because the sulfate ions remained on the titania surface. The bond formation between the dye molecule and the titanium species on the titania surface, i.e., the dye–titania complex formation, enhanced the electron injection from the dye to the titania conduction band.

Acknowledgements This work has been supported by JSPS KAKENHI Grant Number 24550153.

REFERENCES

1. Maeda, M. (1984) Laser Dyes: Properties of Organic Compounds for Dye Lasers. Academic Press, Tokyo, Japan.
2. Grätzel, M. (2003) Dye-sensitized solar cells. J. Photochem. Photobiol. C 4, 145−153.
3. El Mekkawi, D. and M. S. A. Abdel-Mottaleb (2005) The interaction and photostability of some xanthenes and selected azo sensitizing dyes with TiO_2 nanoparticles. Int. J. Photoenergy 7, 95−101.

4. Sharma, G. D., P. Balraju, M. Kumar and M. S. Roy (2009) Quasi solid state dye sensitized solar cells employing a polymer electrolyte and xanthene dyes. Mater. Sci. Eng. B 162, 32−39.
5. Dislich, H. (1971) New Routes to Multicomponent Oxide Glasses. Angew. Chem., Int. Ed. Engl. 10, 363−370.
6. Dislich, H. (1983) Glassy and Crystalline Systems from Gels: Chemical Basis and Technical Application. J. Non-Cryst. Solids 57, 371−388.
7. Brinker, C. J. and G. W. Scherer (1990) Sol–Gel Science: The Physics and Chemistry of Sol–Gel Processing. Academic Press, San Diego.
8. Brinker, C. J., G. C. Frye, A. J. Hurd and C. S. Ashley (1991) Fundamentals of sol–gel dip coating. Thin Solid Films 201, 97−108.
9. Brinker, C. J., A. J. Hurd, G. C. Frye, P. R. Schunk and C. S. Ashley (1991) Sol–gel thin film formation. J. Ceram. Soc. Jpn. 99, 862−877.
10. Avnir , D., D. Levy and R. Reisfeld (1984) The nature of the silica cage as reflected by spectral changes and enhanced photostability of trapped rhodamine 6G. J. Phys. Chem. 88, 5956−5959.
11. Reisfeld, R., R. Zusman, Y. Cohen and M. Eyal (1988) The spectroscopic behaviour of rhodamine 6G in polar and non-polar solvents and in thin glass and PMMA films. Chem. Phys. Lett. 147, 142−147.
12. Fujii, T., A. Ishii and M. Anpo (1990) Absorption and fluorescence spectra of rhodamine B molecules encapsulated in silica gel networks and their thermal stability. J. Photochem. Photobiol. A 54, 231−237.
13. Narang, U., F. V. Bright and P. N. Prasad (1993) Characterization of rhodamine 6G-doped thin sol–gel films. Appl. Spectrosc. 47, 229−234.
14. Chang, P. H., H. C. Tsai, Y. R. Chen, J. Y. Chen and G. H. Hsiue (2008) Thermal stability

and structural characterization of organic/inorganic hybrid nonlinear optical material containing a two-dimensional chromophore. Langmuir 24, 11921−11927.

15. Fujii, T., H. Nishikiori and T. Tamura (1995) Absorption-spectra of rhodamine-B dimers in dip-coated thin-films prepared by the sol−gel method. Chem. Phys. Lett. 233, 424−429.
16. Nishikiori H. and T. Fujii (1997) Molecular forms of rhodamine B in dip-coated thin films. J. Phys. Chem. B 101, 3680−3687.
17. Nishikiori, H., S. Nagaya, N. Tanaka, A. Katsuki and T. Fujii (1999) Acid−base and monomer−dimer equilibria of methylene blue in dip-coated thin films. Bull. Chem. Soc. Jpn. 72, 915−921.
18. Nishikiori, H., N. Tanaka, Y. Minami, A. Katsuki and T. Fujii (2010) Molecular forms and fluorescence processes of 9-aminoacridine in thin sol−gel films. J. Photochem. Photobiol. A 212, 62−67.
19. Murakoshi, K., G. Kano, Y. Wada, S. Yanagida, H. Miyazaki, M. Matsumoto and S. Murasawa (1995) Importance of binding states between photosensitizing molecules and the TiO_2 surface for efficiency in a dye-sensitized solar cell. J. Electroanal. Chem. 396, 27−34.
20. Kalyanasundaram, K. and M. Grätzel (1998) Applications of functionalized transition metal complexes in photonic and optoelectronic devices. Coord. Chem. Rev. 177, 347−414.
21. He, J., F. Chen, J. Zhao and H. Hidaka (1998) Adsorption model of ethyl ester of fluorescein on colloidal TiO_2 and the mechanism of the interfacial electron transfer. Colloids Surf. A 142, 49−57.

22. Wang, C., C. Liu, Y. Wang and T. Shen (1998) Spectral characteristics and photosensitization effect on TiO_2 of fluorescein in AOT reversed micelles. J. Colloid Interface Sci. 197, 126−132.

23. Hilgendorff, M. and V. Sundström (1998) Dynamics of electron injection and recombination of dye-sensitized TiO_2 particles. J. Phys. Chem. B 102, 10505−10514.

24. Ramakrishna, G. and H. N. Ghosh (2001) Emission from the charge transfer state of xanthene dye-sensitized TiO_2 nanoparticles: a new approach to determining back electron transfer rate and verifying the marcus inverted regime. J. Phys. Chem. B 105, 7000−7008.

25. Benkö, G., M. Hilgendorff, A. P. Yartsev and V. Sundström (2001) Electron injection and recombination in fluorescein 27-sensitized TiO_2 thin films. J. Phys. Chem. B 105, 967−974.

26. Benkö, G., B. Skårman, R. Wallenberg, A. Hagfeldt, V. Sundström and A. P. Yartsev (2003) Particle size and crystallinity dependent electron injection in fluorescein 27-sensitized TiO_2 films. J. Phys. Chem. B 107, 1370−1375.

27. Pelet, S., M. Grätzel and J. E. Moser (2003) Femtosecond dynamics of interfacial and intermolecular electron transfer at eosin-sensitized metal oxide nanoparticles. J. Phys. Chem. B 107, 3215−3224.

28. Ramakrishna, G., A. Das and H. N. Ghosh (2004) Effect of surface modification on back electron transfer dynamics of dibromo fluorescein sensitized TiO_2 nanoparticles. Langmuir 20, 1430−1435.

29. Nishikiori, H., N. Tanaka, T. Kitsui and T. Fujii (2006) Photocurrent observed in dye-doped titania gel. J. Photochem. Photobiol. A 179, 125−129.

30. Kitsui, T., H. Nishikiori, N. Tanaka and T. Fujii (2006) Effect of steam treatment on photocurrent and dye–titania interaction in dye-doped titania gel. J. Photochem. Photobiol. A 192, 220−225.

31. Nishikiori, H., W. Qian, M. A. El-Sayed, N. Tanaka and T. Fujii (2007) Change in titania structure from amorphousness to crystalline increasing photoinduced electron-transfer rate in dye-titania system. J. Phys. Chem. C 111, 9008−9011.

32. Nishikiori, H., Y. Uesugi, N. Tanaka and T. Fujii (2009) Photo-electric conversion in dye-doped nanocrystalline titania films. J. Photochem. Photobiol. A 207, 204−208.

33. Nishikiori, H., Y. Uesugi, S. Takami, R. A. Setiawan, T. Fujii, W. Qian and M. A. El-Sayed (2011) Influence of steam treatment on dye−titania complex formation and photoelectric conversion property of dye-doped titania gel. J. Phys. Chem. C 115, 2880−2887.

34. Nishikiori, H., Y. Uesugi, R. A. Setiawan, T. Fujii, W. Qian and M. A. El-Sayed (2012) Photoelectric conversion properties of dye-sensitized solar cells using dye-dispersing titania. J. Phys. Chem. C 116, 4848−4854.

35. Nishikiori, H., R. A. Setiawan, K. Miyamoto, G. Sukmono, Y. Uesugi, K. Teshima and T. Fujii (2012) Photoinduced electron transport in dye-containing titania gel films. RSC Adv. 2, 4258−4267.

36. Setiawan, R. A., H. Nishikiori, Y. Uesugi, K. Miyashita, M. A. El-Sayed and T. Fujii (2013) Electron transfer process in fluorescein-dispersing titania gel films observed by time-resolved fluorescence spectroscopy. J. Phys. Chem. C 117, 10308−10314.

37. Nishikiori, H., R. A. Setiawan, K. Miyashita, K. Teshima and T. Fujii (2013) Influence of dye dispersion on photoelectric conversion properties of dye-containing titania electrodes. Catal. Sci. Technol. 3, 1512−1519.

38. Yanagisawa, K. and J. Ovenstone (1999) Crystallization of anatase from amorphous titania using the hydrothermal technique: effects of starting material and temperature. J. Phys. Chem. B 103, 7781−7787.

39. Khazraji, A. C., S. Hotchandani, S. Das and P. V. Kamat (1999) Controlling dye (merocyanine-540) aggregation on nanostructured TiO_2 films. An organized assembly approach for enhancing the efficiency of photosensitization. J. Phys. Chem. B 103, 4693−4700.

40. Keis, K., J. Lindgren, S. Lindquist and A. Hagfeldt (2000) Studies of the adsorption process of Ru Complexes in manoporous ZnO electrodes. Langmuir 16, 4688−4694.

41. Wenger, B., M. Grätzel and J. Moser (2005) Rationale for kinetic heterogeneity of ultrafast light-induced electron transfer from Ru(II) complex sensitizers to nanocrystalline TiO_2. J. Am. Chem. Soc. 127, 12150−12151.

42. Wang, L., A. Roitberg, C. Meuse and A. K. Gaigalas (2001) Raman and FTIR spectroscopies of fluorescein in solutions. Spectrochim. Acta, A 57, 1781−1791.

43. Aguado-Serrano, J. and M. L. Rojas-Cervantes (2006) Titania aerogels influence of synthesis parameters on textural, crystalline, and surface acid properties. Micropor. Mesopor. Mater. 88, 205−213.

44. Colón, G., J. M. Sánchez-España, M. C. Hidalgo and J. A. Navío (2006) Effect of TiO_2 acidic pre-treatment on the photocatalytic properties for phenol degradation. J. Photochem. Photobiol. A 179, 20−27.

45. Mchedlov-Petrossyan, N. O. and V. N. Kleshchevnikova (1994) Influence of the cetyltrimethylammonium chloride micellar pseudophase on the protolytic equilibria of

oxyxanthene dyes at high bulk phase ionic strength. J. Chem. Soc., Faraday Trans. 90, 629−640.

46. Kim, B., S. W. Park, J. Y. Kim, K. Yoo, J. A. Lee, M. W. Lee, D. K. Lee, J. Y. Kim, B. Kim, H. Kim, S. Han, H. J. Son and M. J. Ko (2013) Rapid dye adsorption via surface modification of TiO_2 photoanodes for dye-sensitized solar cells. ACS Appl. Mater. Interfaces 5, 5201−5207.

47. Fujii, T., A. Ishii, N. Takusagawa and M. Anpo (1992) Fluorescence spectra and chemical species of fluorescein molecules adsorbed on a calcinated porous vycor glass. Res. Chem. Intermed. 17, 1−14.

48. Nishikiori, H., R. A. Setiawan, S. Kawamoto, S. Takagi,, K. Teshima and T. Fujii (2013) Dimerization of xanthene dyes in sol–gel titania films. Catal. Sci. Technol. 3, 2786−2792.

49. Sjöback, R., J. Nygren and M. Kubista (1995) Absorption and fluorescence properties of fluorescein. Spectrochim. Acta, A 51, L7–L21.

50. Magde, D., R. Wong and P. G. Seybold (2002) Fluorescence quantum yields and their relation to lifetimes of rhodamine 6G and fluorescein in nine solvents: improved absolute standards for quantum yields. Photochem. Photobiol. 75, 327–334.

51. Du, L., A. Furube, K. Hara, R. Katoh and M. Tachiya (2010) Mechanism of particle size effect on electron injection efficiency in ruthenium dye-sensitized TiO_2 nanoparticle films. J. Phys. Chem. C 114, 8135−8143.

52. Asbury, J. B., N. A. Anderson, E. Hao, X. Ai and T. Lian (2003) Parameters affecting electron injection dynamics from ruthenium dyes to titanium dioxide nanocrystalline thin film. J. Phys. Chem. B 107, 7376–7386.

53. Benkö, G., J. Kallioinen, J. E. I. Korppi-Tommola, A. P. Yartsev and V. Sundström

(2002) Photoinduced ultrafast dye-to-semiconductor electron injection from nonthermalized and thermalized donor states. J. Am. Chem. Soc. 124, 489–493.

54. Eder, D. and R. Kramer (2003) Stoichiometry of “titanium suboxide”. Part 2. Electric properties. Phys. Chem. Chem. Phys. 5, 1314–1319.
55. Nishikiori, H., Y. Uesugi, R. A. Setiawan and K. Teshima (2012) Photoelectric conversion properties of dye-sensitized solar cell electrodes with dye-dispersing titania layers. J. Soc. Inorg. Mater. Jpn. 19, 237–242.
56. Kunimatsu, K, M. G. Samant, H. Seki and M. R. Philpott (1988) A study of HSO_4^- and SO_4^{2-} co-adsorption on a platinum electrode in sulfuric acid by in-situ FT-IR reflection absorption spectroscopy. J. Electroanal. Chem. 243, 203–208.
57. Wang, X., J. C. Yu, P. Liu, X. Wang, W. Su and X. Fu (2006) Probing of photocatalytic surface sites on SO_4^{2-}/TiO_2 solid acids by in situ FT-IR spectroscopy and pyridine adsorption. J. Photochem. Photobiol. A 179, 339–347.

Table 1. Concentrations (/ mol dm^{-3}) of the neutral, anion, and dianion species of fluorescein in the untreated films, F-1NF, F-2NF, and F-3NF, and those steam-treated for 120 min, F-1NF-s, F-2NF-s, and F-3NF-s.

	Neutral	Anion	Dianion	Total
F-1NF	0.275 (32.6%)	0.526 (62.4%)	0.0425 (5.0%)	0.843
F-2NF	0.131 (26.1%)	0.364 (72.5%)	0.00705 (1.4%)	0.502
F-3NF	0.118 (37.4%)	0.194 (61.5%)	0.00333 (1.1%)	0.315
F-1NF-s	0.00942 (9.2%)	0.0868 (84.6%)	0.00632 (6.2%)	0.102
F-2NF-s	0.0648 (27.5%)	0.164 (69.5%)	0.00717 (3.0%)	0.236
F-3NF-s	0.0179 (27.5%)	0.0459 (70.5%)	0.00131 (2.0%)	0.0201

Figure captions

Figure 1. SEM images of the surface morphology of the electrodes steam-treated for 120 min, (a) WE-1NF-s, (b) WE-2NF-s, and (c) WE-3NF-s.

Figure 2. XRD patterns of the films untreated, (1) F-2NF, and steam-treated for 120 min, (2) F-1NF-s, (3) F-2NF-s, and (4) F-3NF-s.

Figure 3. FTIR spectra of (a) the untreated films, (1) F-1NF, (2) F-2NF, and (3) F-3NF, and (b) those steam-treated for 120 min, (1) F-1NF-s, (2) F-2NF-s, and (3) F-3NF-s.

Figure 4. (a) Visible absorption spectra of the sol−gel reaction systems, (1) SG-1NF, (2) SG-2NF, and (3) SG-3NF, in which the reaction proceeded for 1 day, and (b) the separated spectra of the (1) neutral, (2) anion, and (3) dianion species of fluorescein.

Figure 5. Visible absorption spectra of (a) the untreated films, (1) F-1NF, (2) F-2NF, and (3) F-3NF, and (b) those steam-treated for 120 min, (1) F-1NF-s, (2) F-2NF-s, and (3) F-3NF-s.

Figure 6. Fluorescence spectra of (a) the untreated films, (1) F-1NF, (2) F-2NF, and (3) F-3NF, and (b) those steam-treated for 120 min, (1) F-1NF-s, (2) F-2NF-s, and (3) F-3NF-s. The excitation wavelength was 500 nm.

Figure 7. Fluorescence quantum yields of the untreated films, (1) F-1NF, (2) F-2NF, and (3) F-3NF, and those steam-treated for 120 min, (1) F-1NF-s, (2) F-2NF-s, and (3) F-3NF-s.

Figure 8. IPCE spectra of (a) the untreated electrodes, (1) WE-1NF, (2) WE-2NF, and (3) WE-3NF, and (b) those steam-treated for 120 min, (1) WE-1NF-s, (2) WE-2NF-s, and (3) WE-3NF-s.

Figure 9. Quantum efficiency of photoelectric conversion at each wavelength for (a) the untreated electrodes, (1) WE-1NF, (2) WE-2NF, and (3) WE-3NF, and (b) those steam-treated for 120 min, (1) WE-1NF-s, (2) WE-2NF-s, and (3) WE-3NF-s.

Figure 10. Fluorescence quantum yields of the untreated films, (1) F-2NF, (2) F-2HF, and (3) F-2SF, and those steam-treated for 120 min, (1) F-2NF-s, (2) F-2HF-s, and (3) F-2SF-s.

Figure 11. Quantum efficiency of photoelectric conversion at 470 nm for the untreated electrodes, (1) WE-2NF, (2) WE-2HF, and (3) WE-2SF, and those steam-treated for 120 min, (1) WE-2NF-s, (2) WE-2HF-s, and (3) WE-2SF-s.

Figure 12. Fluorescence quantum yield and quantum efficiency of photoelectric conversion for the (a) untreated and (b) steam-treated electrodes vs. the dianion fraction of fluorescein.

Figure 1

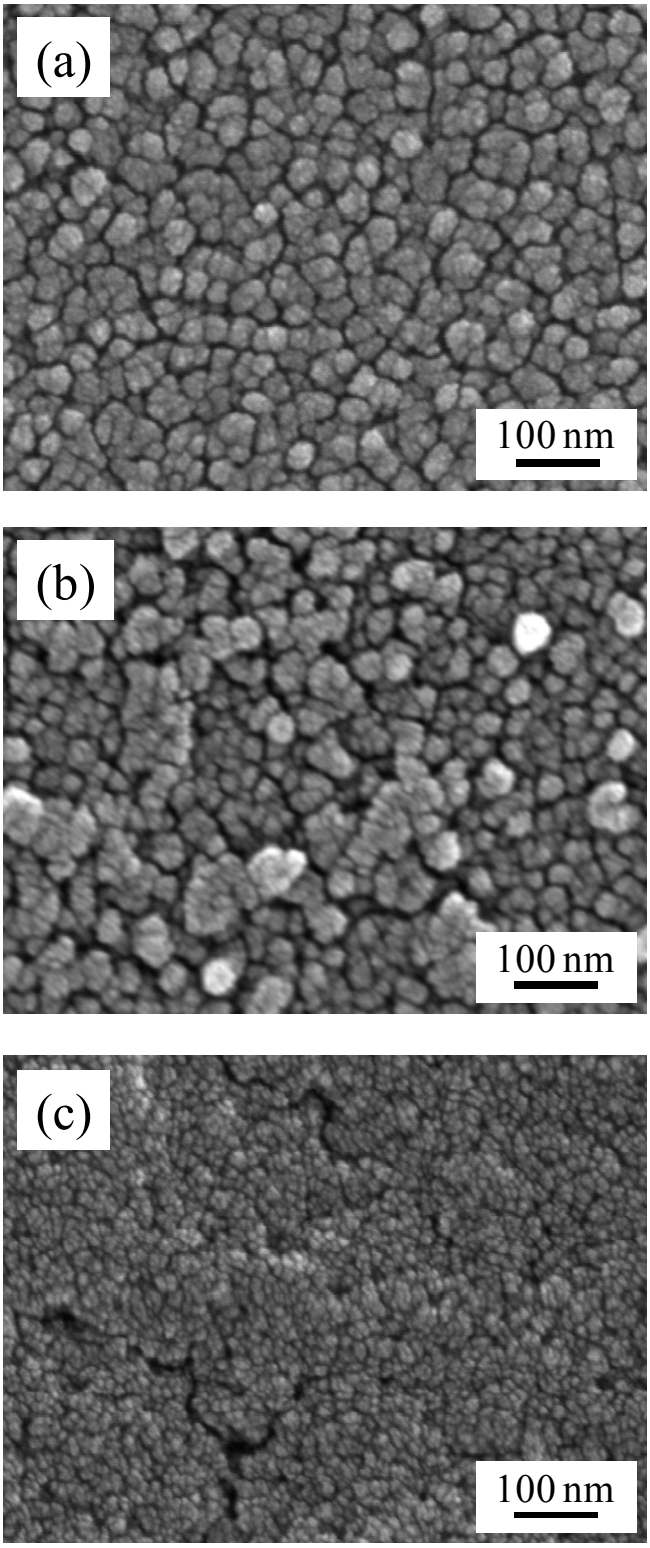

Figure 2

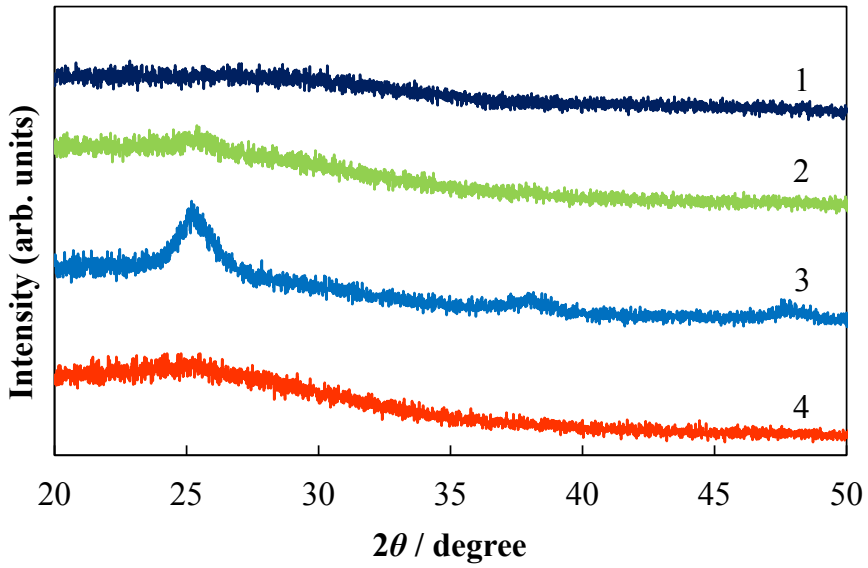

Figure 3

(a)

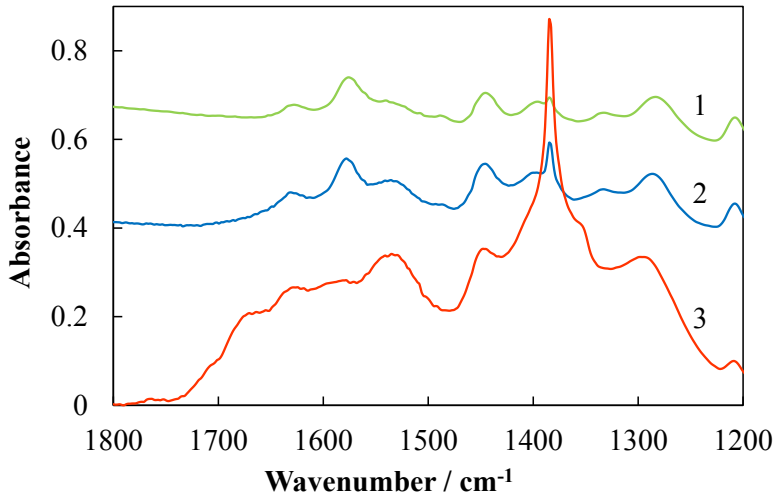
0.8
0.6
0.4
0.2
0
Absorbance
1
2
3
1800
1700
1600
1500
1400
1300
1200
Wavenumber / cm-1

(b)

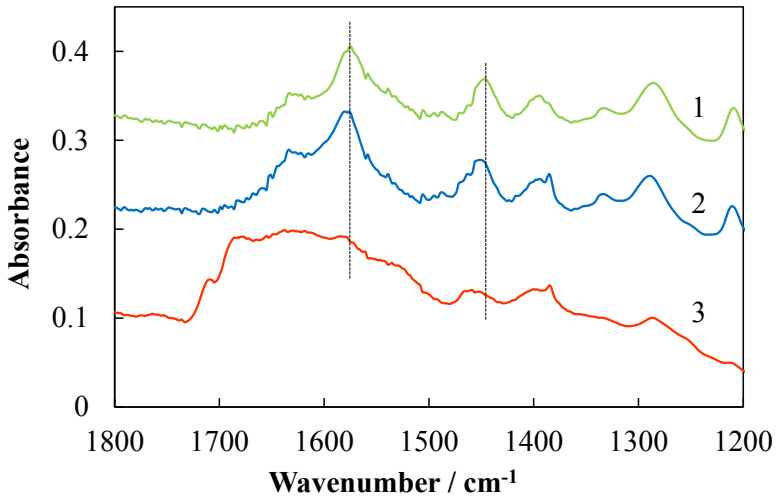
0.4
0.3
0.2
0.1
0
Absorbance
1
2
3
1800
1700
1600
1500
1400
1300
1200
Wavenumber / cm-1

Figure 4

(a)

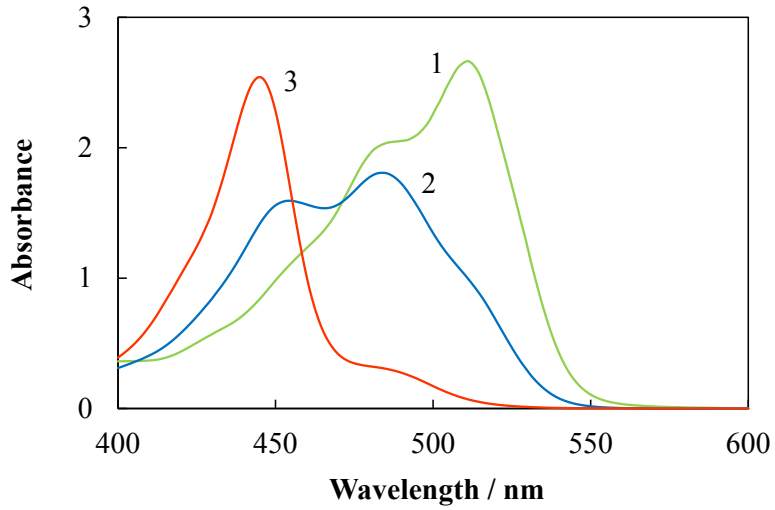
Absorbance
Wavelength / nm
1
2
3

(b)

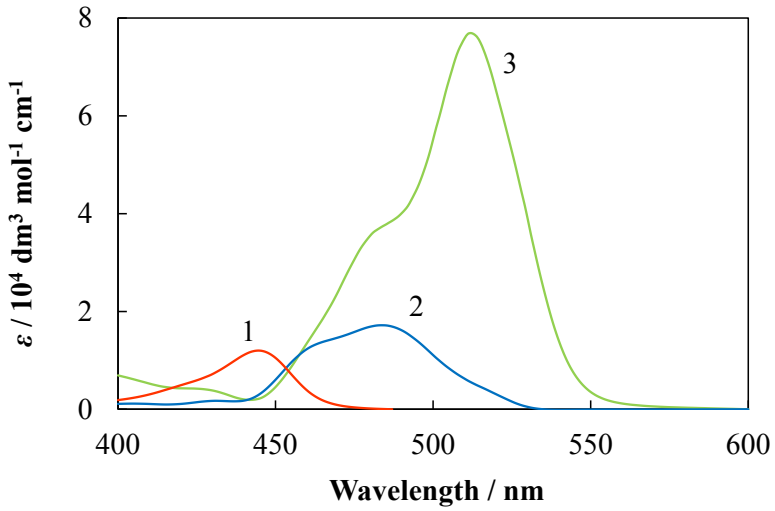
ε / 10⁴ dm³ mol⁻¹ cm⁻¹
Wavelength / nm
1
2
3

Figure 5

(a)

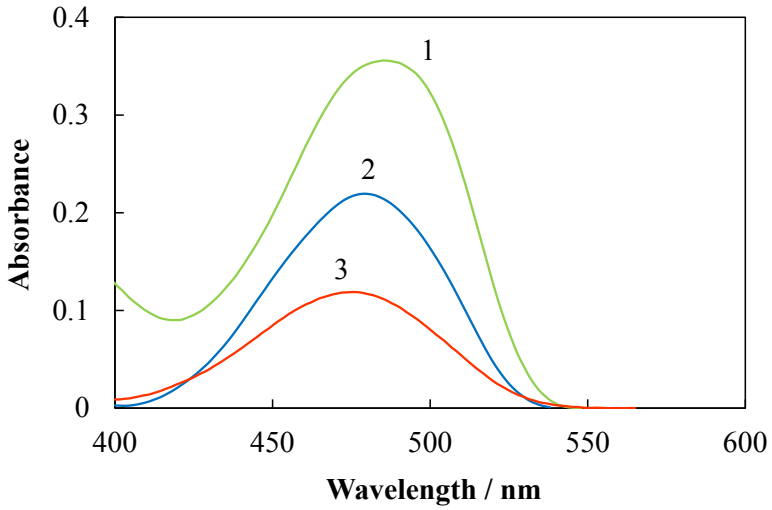
0.4
0.3
0.2
0.1
0
Absorbance
1
2
3
400
450
500
550
600
Wavelength / nm

(b)

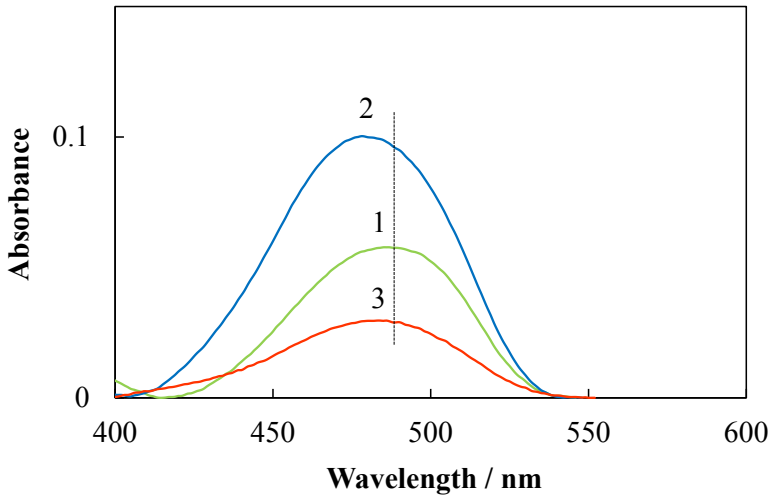
0.1
0
Absorbance
2
1
3
400
450
500
550
600
Wavelength / nm

Figure 6

(a)

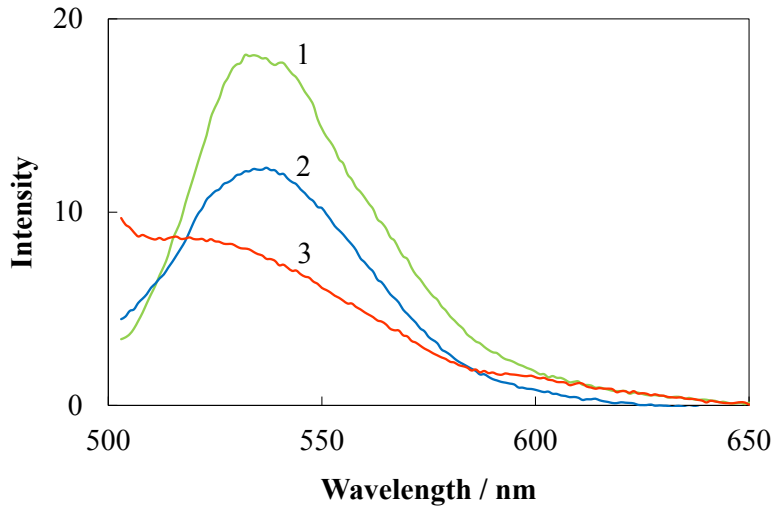
20
10
0
Intensity
1
2
3
500
550
600
650
Wavelength / nm

(b)

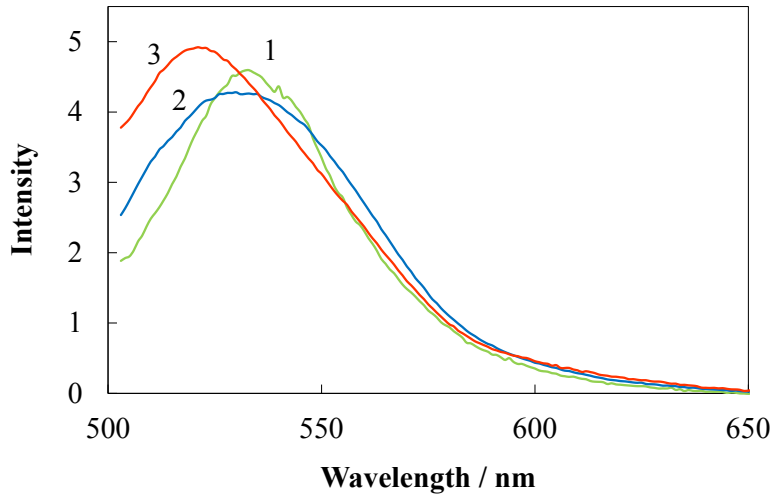
5
4
3
2
1
0
Intensity
3
1
2
500
550
600
650
Wavelength / nm

Figure 7

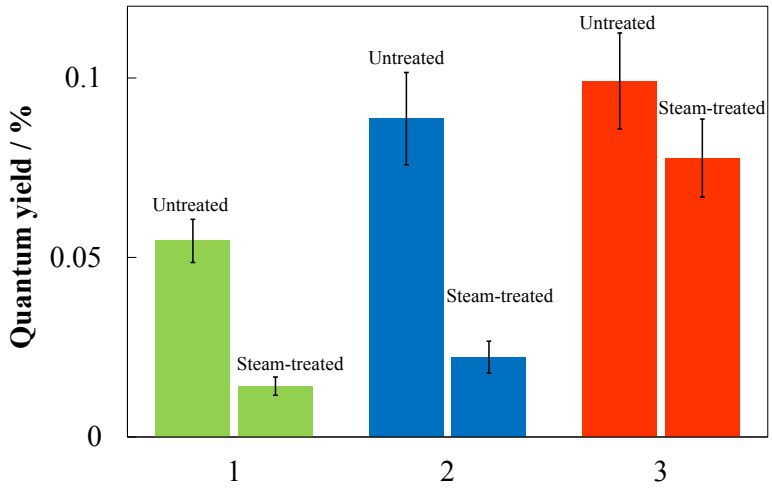
Quantum yield / %
0.1
0.05
0
Untreated
Steam-treated
Untreated
Steam-treated
Untreated
Steam-treated
1
2
3

Figure 8

(a)

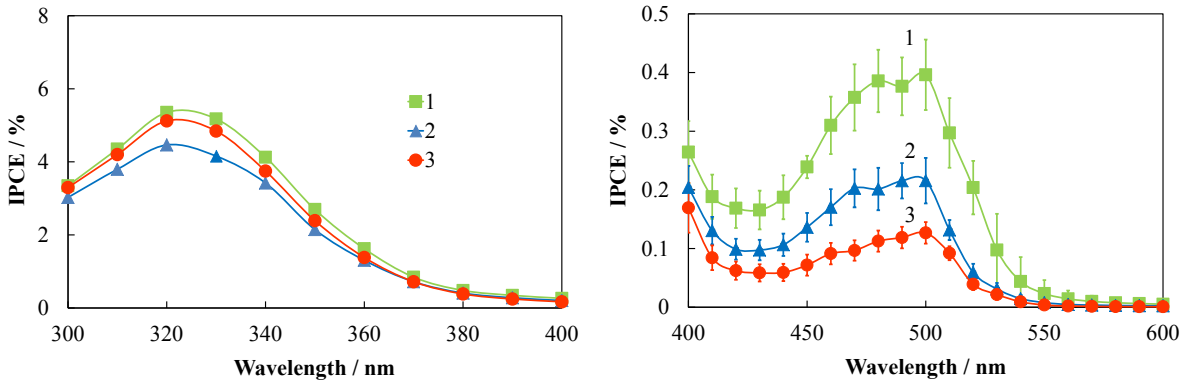

(b)

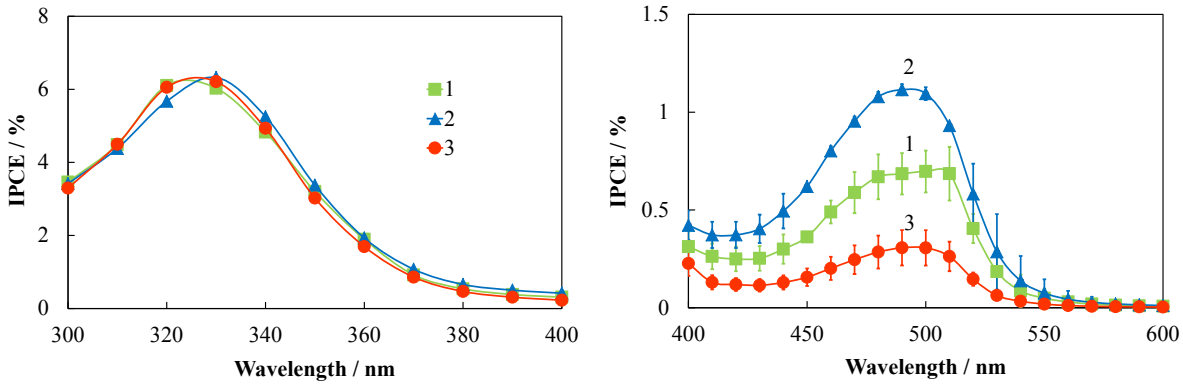

Figure 9

(a)

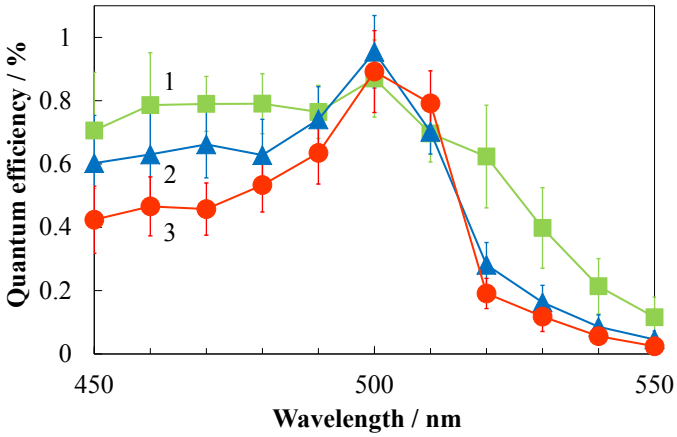
Quantum efficiency / %
1
0.8
0.6
0.4
0.2
0
1
2
3
450
500
550
Wavelength / nm

(b)

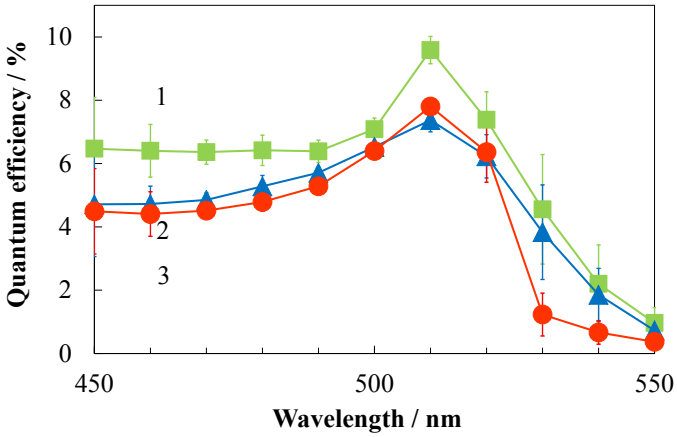
Quantum efficiency / %
10
8
6
4
2
0
1
2
3
450
500
550
Wavelength / nm

Figure 10

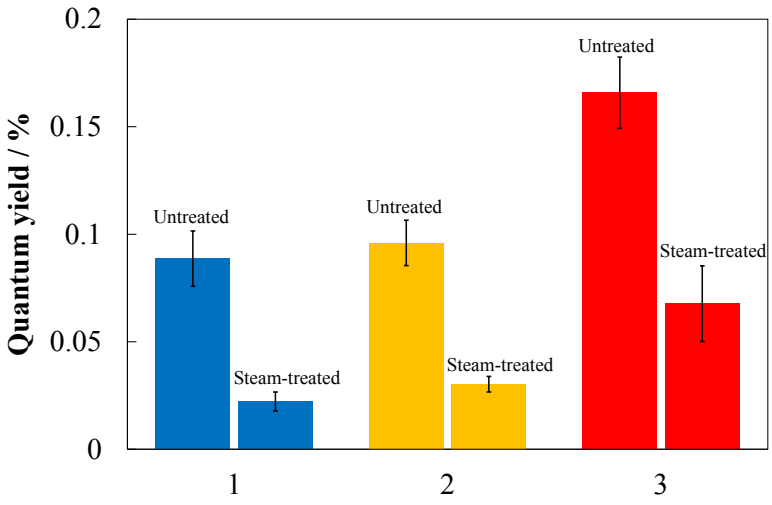
Quantum yield / %
0.2
0.15
0.1
0.05
0
Untreated
Steam-treated
Untreated
Steam-treated
Untreated
Steam-treated
1
2
3

Figure 11

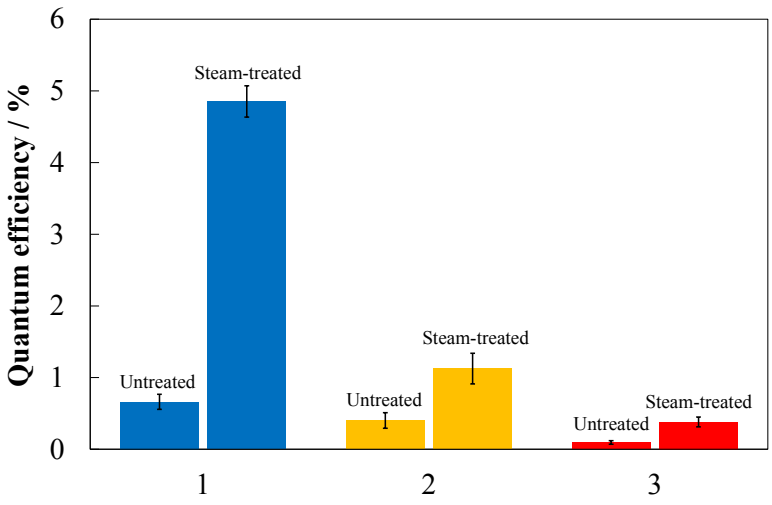
Quantum efficiency / %
6
5
4
3
2
1
0
Steam-treated
Untreated
Steam-treated
Untreated
Steam-treated
Untreated
1
2
3

Figure 12

(a)

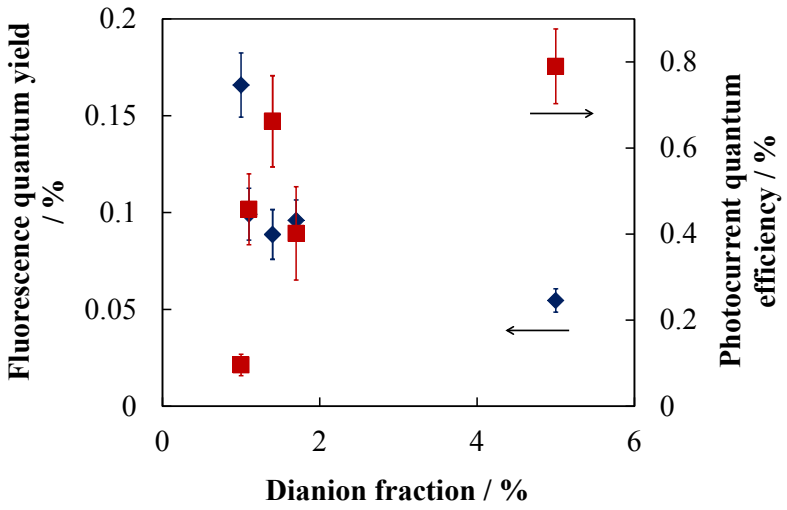
Fluorescence quantum yield / %
0.2
0.15
0.1
0.05
0
0
2
4
6
Dianion fraction / %
0.8
0.6
0.4
0.2
0
Photocurrent quantum efficiency / %

(b)

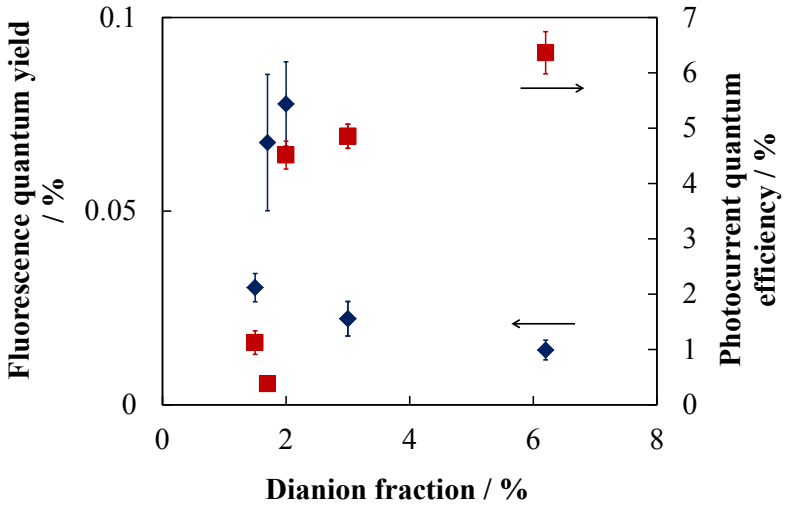
Fluorescence quantum yield / %
0.1
0.05
0
0
2
4
6
8
Dianion fraction / %
7
6
5
4
3
2
1
0
Photocurrent quantum efficiency / %

SUPPORTING INFORMATION

(a)

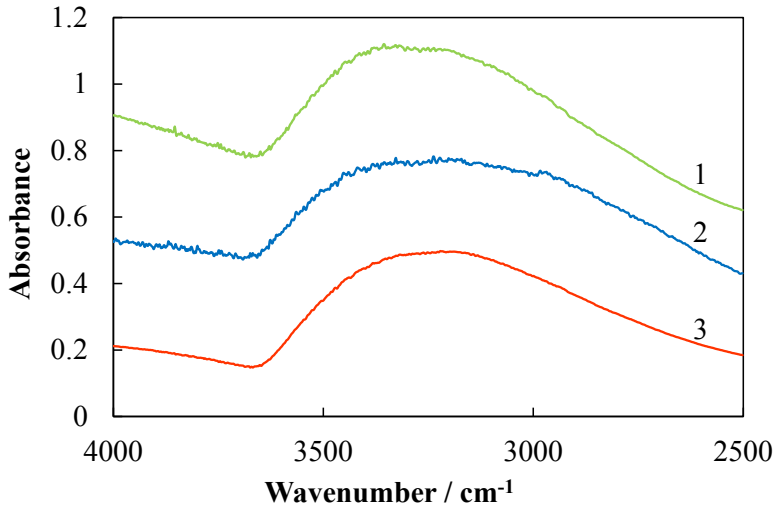

(b)

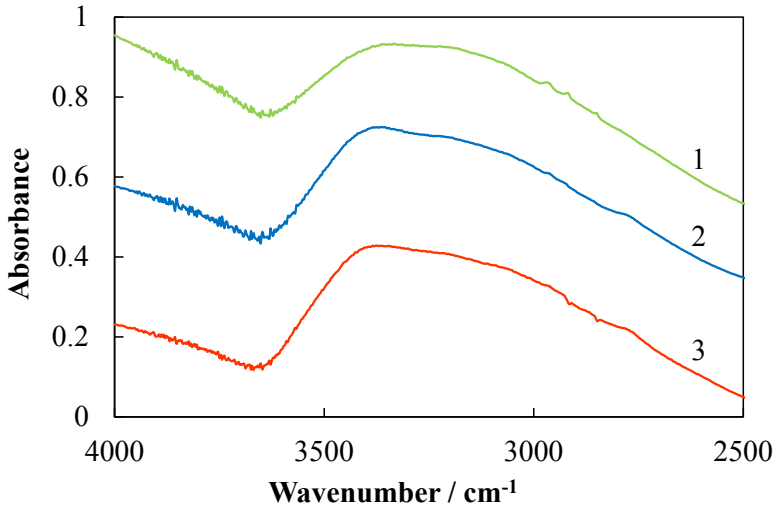

Figure S1. FTIR spectra (4000−2500 cm^{-1}) of (a) the untreated films, (1) F-1NF, (2) F-2NF, and (3) F-3NF, and (b) those steam-treated for 120 min, (1) F-1NF-s, (2) F-2NF-s, and (3) F-3NF-s.

(a)

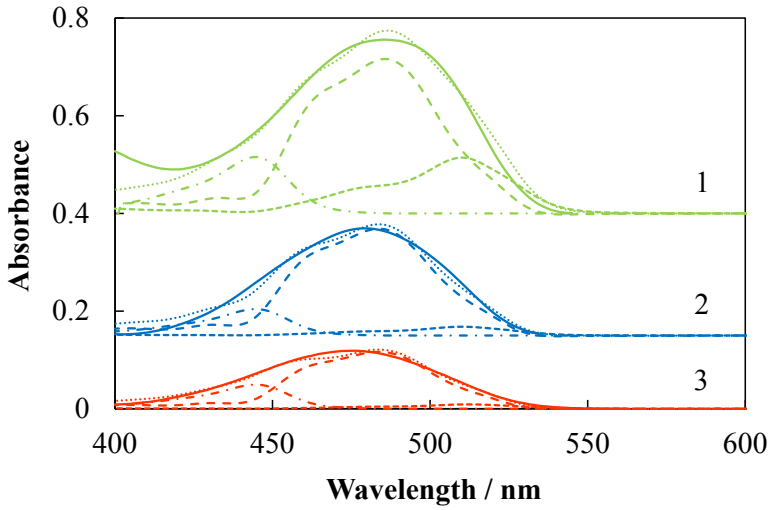

(b)

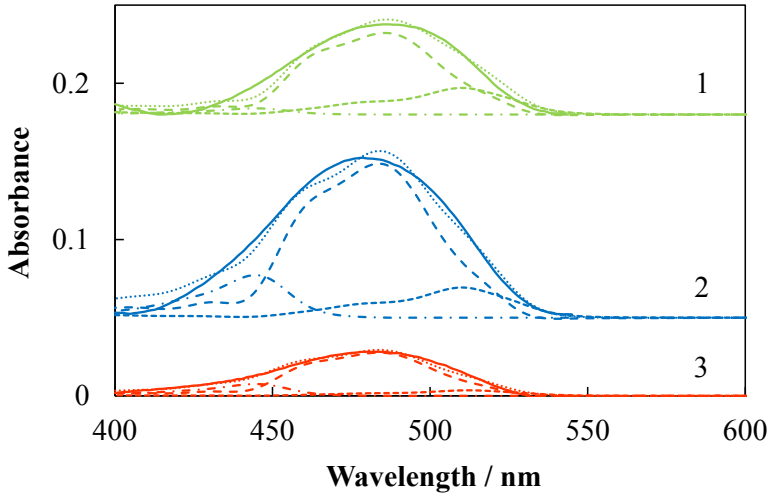

Figure S2. Visible absorption spectra and the separated constituent spectra of (a) the untreated films, (1) F-1NF, (2) F-2NF, and (3) F-3NF, and (b) those steam-treated for 120 min, (1) F-1NF-s, (2) F-2NF-s, and (3) F-3NF-s.

(a)

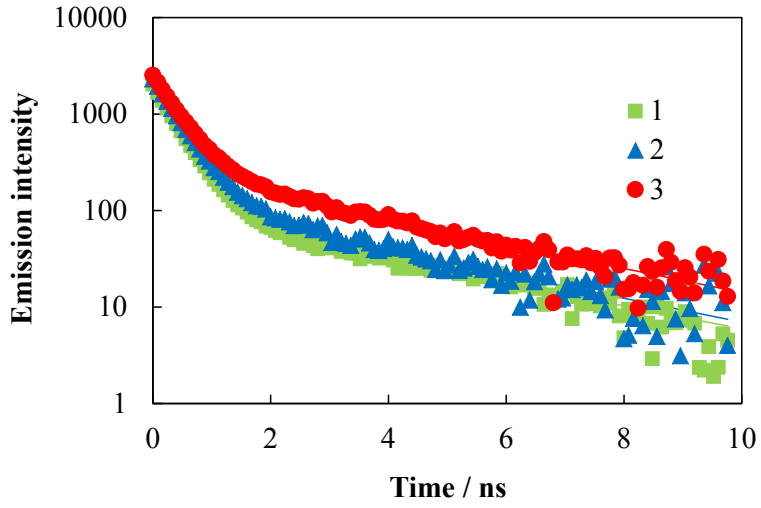

(b)

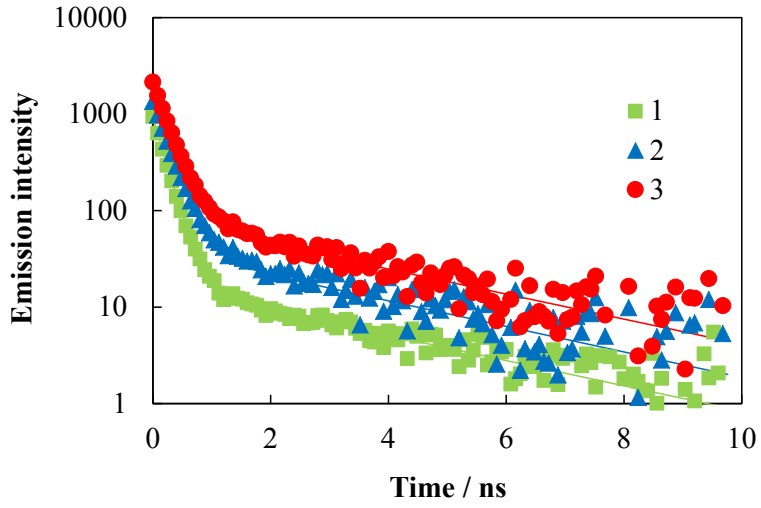

Figure S3. Fluorescence decay profiles of (a) the untreated films, (1) F-1NF, (2) F-2NF, and (3) F-3NF, and (b) those steam-treated for 120 min, (1) F-1NF-s, (2) F-2NF-s, and (3) F-3NF-s.

A Ti:Sapphire femtosecond pulse laser and streak scope spectroscopic system were used for the time-resolved fluorescence measurements in order to obtain information about the fluorescence quenching due to the electron injection from the dye to the titania. The laser system (Clark MXR CPA 2001) generates laser pulses of 150 fs duration (FWHM) with an energy of 750 μJ at 750 nm and a repetition rate of 1 kHz. The second harmonics of the

laser pulses (375 nm) was used for the excitation. The fluorescence signal was monitored using a streak scope system (Hamamatsu Photonics C4780). The fluorescence decay curves were obtained by integrating the fluorescence signals in the 500–550 nm region. The film samples for this measurement were washed with a 0.1 mol dm^{-3} sodium hydroxide aqueous solution and water in order to adjust to the same amount of the dye. The amount of the dye was confirmed by a UV-visible absorption measurement.

Table S1. Emission intensity and fitting parameters of the time-resolved fluorescence of (a) the untreated films, (1) F-1NF, (2) F-2NF, and (3) F-3NF, and (b) those steam-treated for 120 min, (1) F-1NF-s, (2) F-2NF-s, and (3) F-3NF-s.

	Maximum intensity	τ_1 / ns	τ_2 / ns	A_1	A_2
F-1NF	2030±70	0.40±0.01	3.7±0.1	0.96±0.01	0.04±0.01
F-2NF	2320±60	0.42±0.01	3.5±0.1	0.95±0.01	0.05±0.01
F-3NF	2540±50	0.43±0.01	3.5±0.1	0.90±0.02	0.10±0.02
F-1NF-s	950±40	0.20±0.01	3.3±0.1	0.98±0.01	0.02±0.01
F-2NF-s	1360±50	0.24±0.01	3.3±0.1	0.97±0.01	0.03±0.01
F-3NF-s	2150±80	0.25±0.01	3.4±0.1	0.96±0.01	0.04±0.01

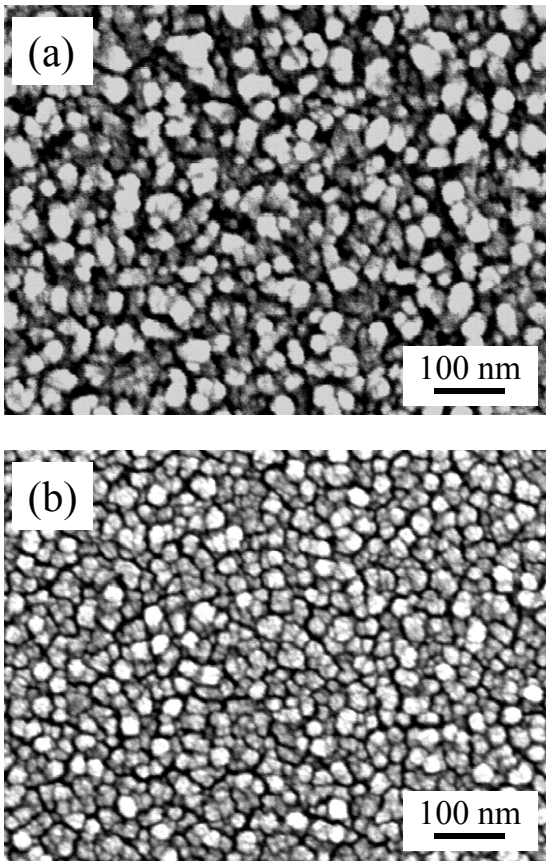

Figure S4. SEM images of the surface morphology of the electrodes steam-treated for 120 min, (a) WE-2HF-s and (b) WE-2SF-s.

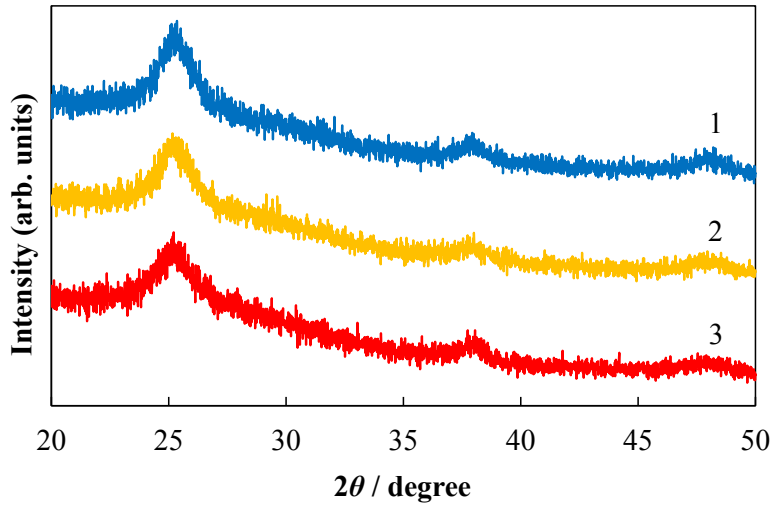

Figure S5. XRD patterns of the films steam-treated for 120 min, (1) F-2NF-s, (2) F-2HF-s, and (3) F-2SF-s.

(a)

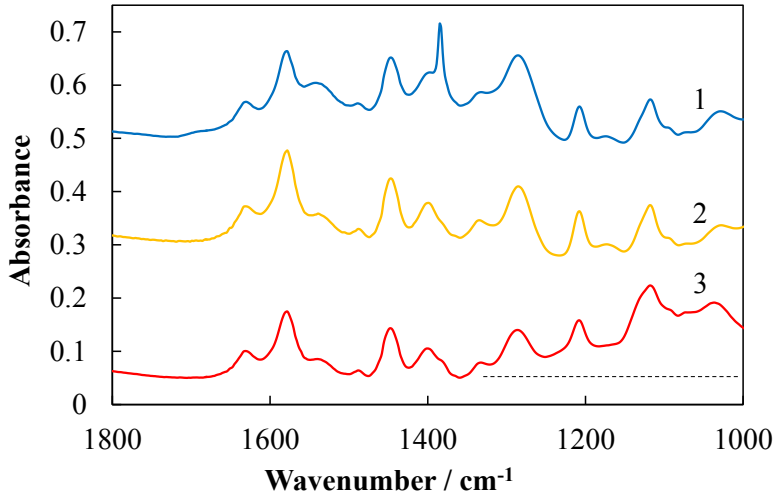

(b)

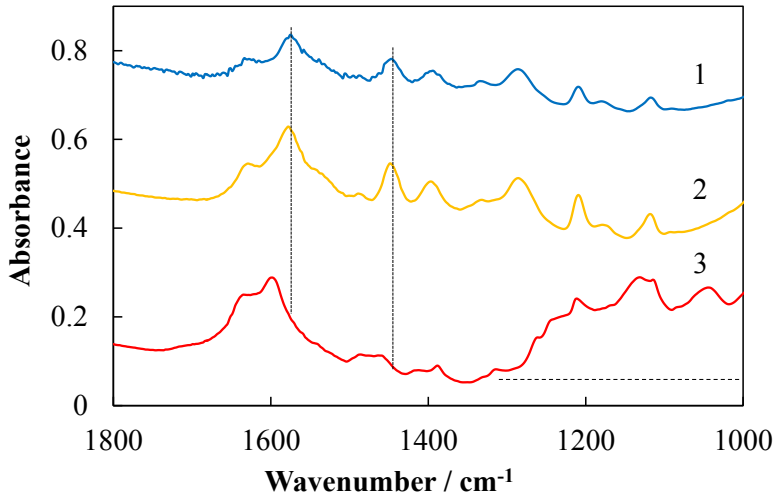

Figure S6. FTIR spectra (1800−1000 cm^{-1}) of (a) the untreated films, (1) F-2NF, (2) F-2HF, and (3) F-2SF, and (b) those steam-treated for 120 min, (1) F-2NF-s, (2) F-2HF-s, and (3) F-2SF-s.

(a)

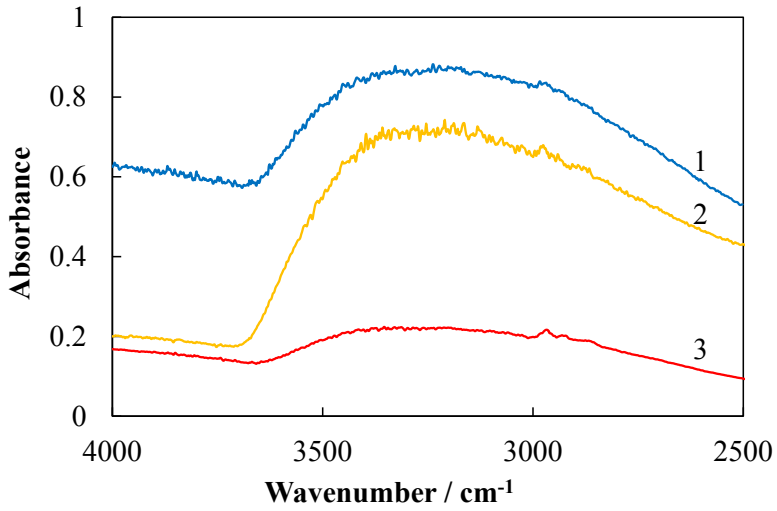

(b)

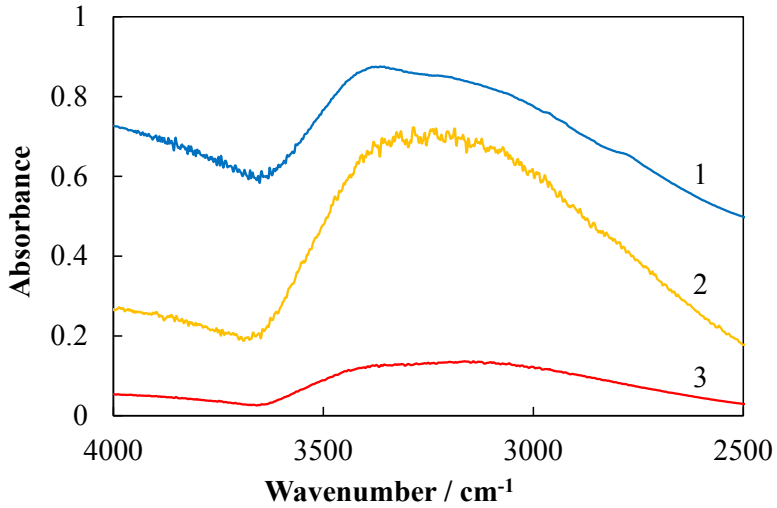

Figure S7. FTIR spectra (4000−2500 cm^{-1}) of (a) the untreated films, (1) F-2NF, (2) F-2HF, and (3) F-2SF, and (b) those steam-treated for 120 min, (1) F-2NF-s, (2) F-2HF-s, and (3) F-2SF-s.

(a)

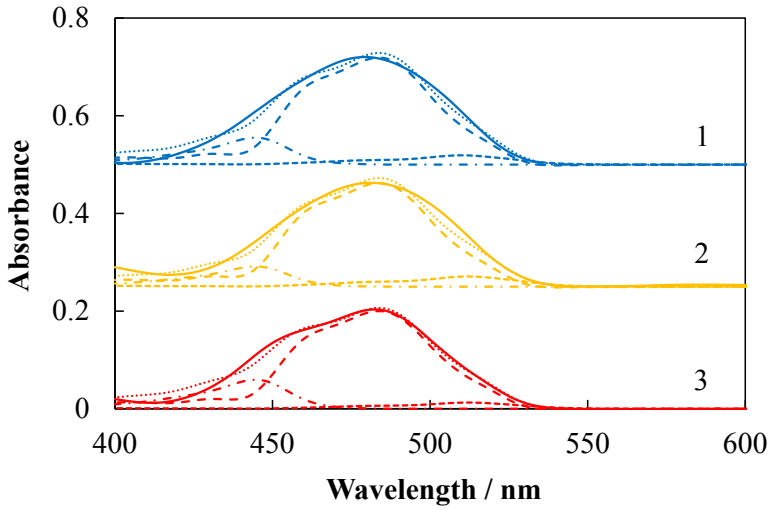

(b)

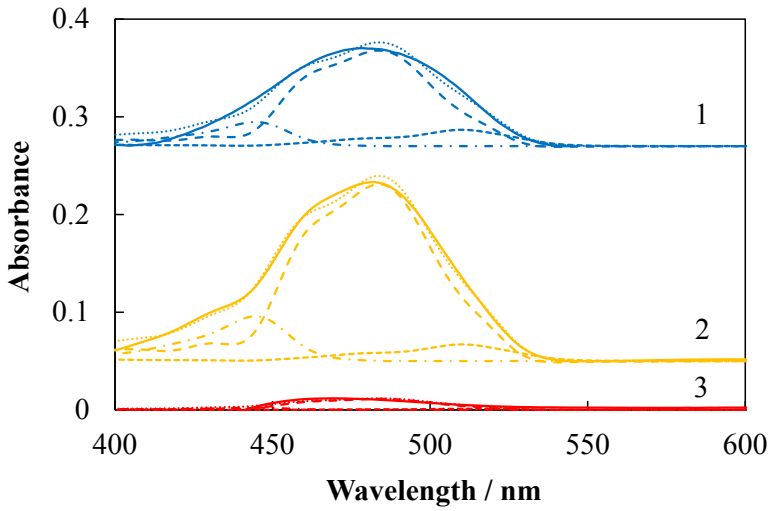

Figure S8. Visible absorption spectra and the separated constituent spectra of (a) the untreated films, (1) F-2NF, (2) F-2HF, and (3) F-2SF, and (b) those steam-treated for 120 min, (1) F-2NF-s, (2) F-2HF-s, and (3) F-2SF-s.

Table S2. Concentrations (/ mol dm^{-3}) of the neutral, anion, and dianion species of fluorescein in the untreated films, F-2NF, F-2HF, and F-2SF, and those steam-treated for 120 min, F-2NF-s, F-2HF-s, and F-2SF-s.

	Neutral	Anion	Dianion	Total
F-2NF	0.131 (26.1%)	0.364 (72.5%)	0.00705 (1.4%)	0.502
F-2HF	0.00986 (21.5%)	0.352 (76.8%)	0.00778 (1.7%)	0.459
F-2SF	0.141 (29.6%)	0.332 (69.5%)	0.00474 (1.0%)	0.479
F-2NF-s	0.00648 (27.5%)	0.164 (69.5%)	0.00717 (3.0%)	0.236
F-2HF-s	0.109 (26.2%)	0.301 (72.3%)	0.00633 (1.5%)	0.416
F-2SF-s	0.00527 (21.6%)	0.0187(76.7%)	0.000420 (1.7%)	0.0244

(a)

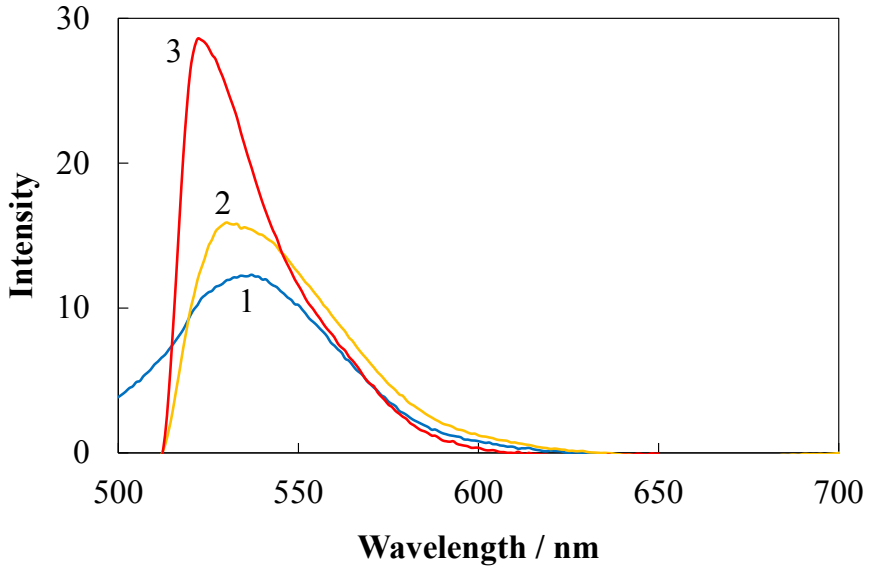

(b)

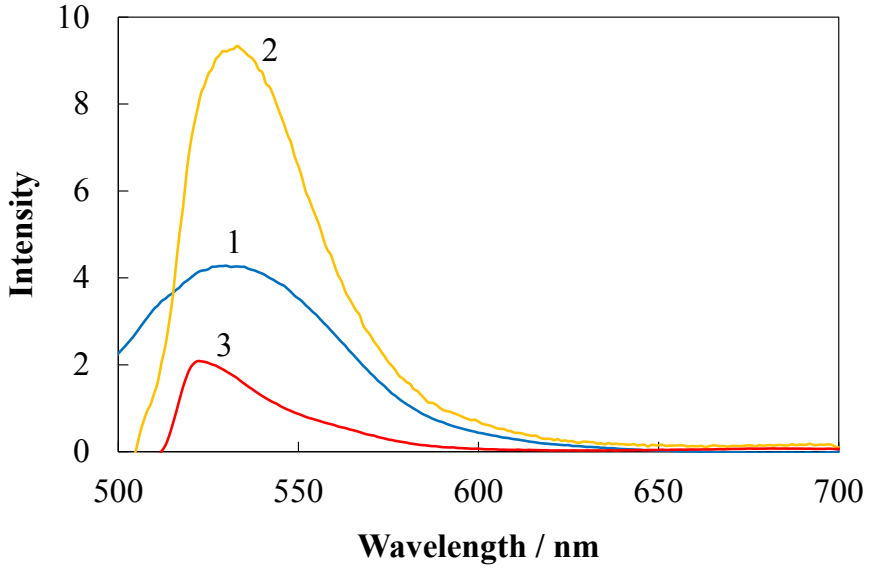

Figure S9. Fluorescence spectra of (a) the untreated films, (1) F-2NF, (2) F-2HF, and (3) F-2SF, and (b) those steam-treated for 120 min, (1) F-2NF-s, (2) F-2HF-s, and (3) F-2SF-s. The excitation wavelength was 500 nm.

(a)

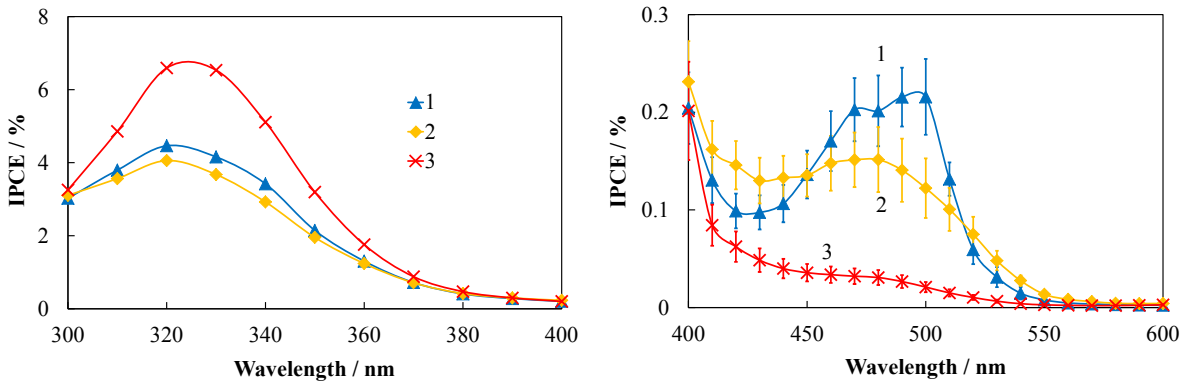

(b)

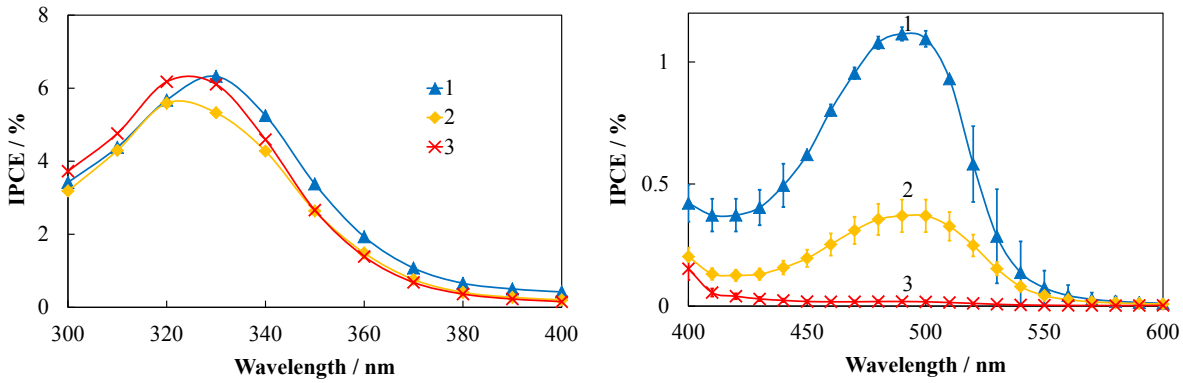

Figure S10. IPCE spectra of (a) the untreated electrodes, (1) WE-2NF, (2) WE-2HF, and (3) WE-2SF, and (b) those steam-treated for 120 min, (1) WE-2NF-s, (2) WE-2HF-s, and (3) WE-2SF-s.

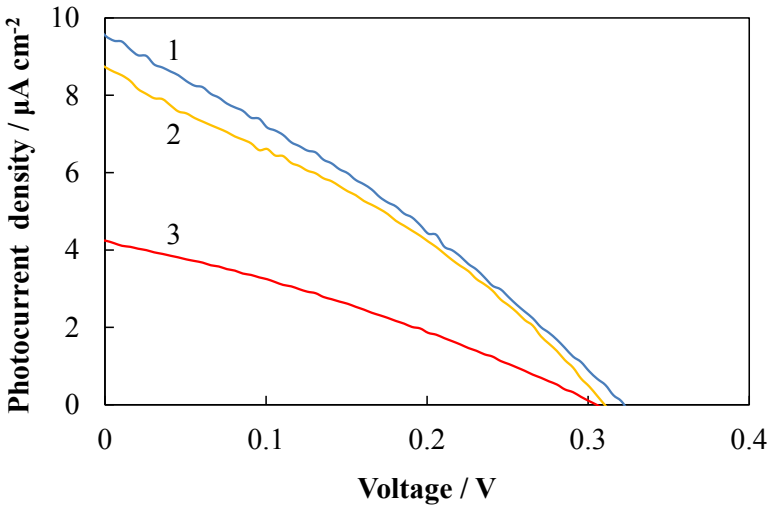

Figure S11. *I*−*V* curves of the untreated electrodes, (1) WE-2NF, (2) WE-2HF, and (3) WE-2SF.

The *I*−*V* curves of the electrodes were measured by a potentiostat (Hokuto Denko HSV-100) during irradiation by the visible light at a wavelength longer than 400 nm emitted by the 150-W Xe short arc lamp using a sharp cut filter.